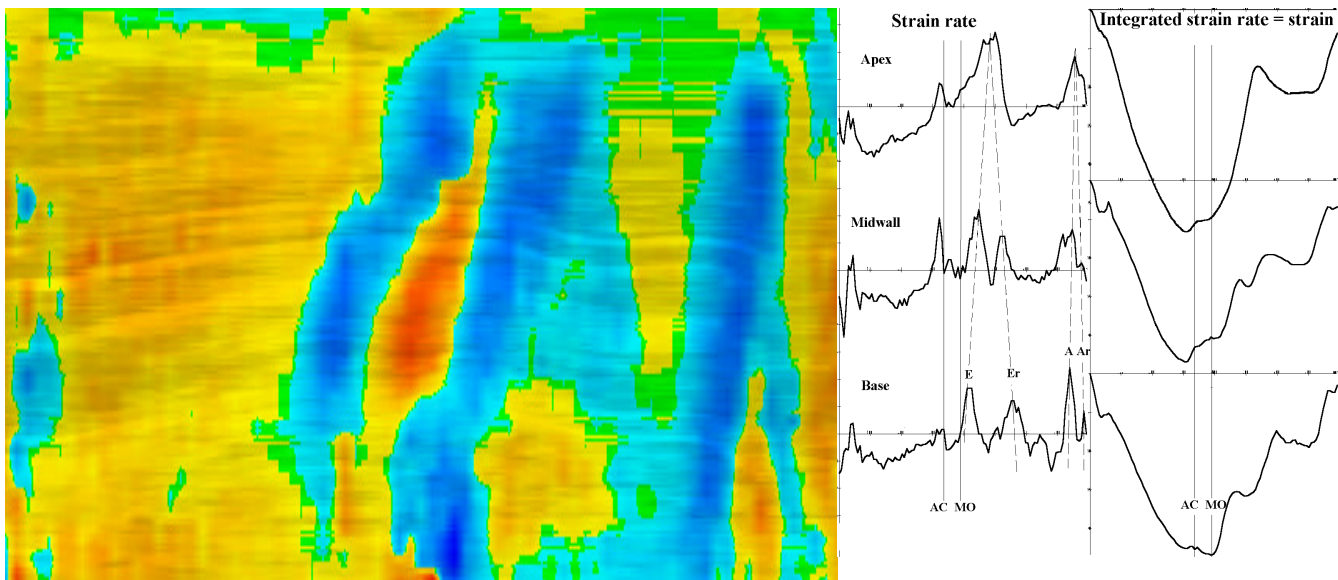


Asbjørn Støylen

Strain rate imaging of the left ventricle by ultrasound.

Feasibility, clinical validation and physiological
aspects.



NTNU
Norwegian University of Science and technology
Faculty of Medicine

Contents:

Acknowledgements.	3
List of Papers.	5
Abbreviations and definitions.	6
1. Introduction.	7
1.1. The concept of strain	7
1.2. Longitudinal motion of the heart	10
1.3. Strain rate	12
1.4. The velocity gradient	12
1.5. Strain Rate Imaging by ultrasound	13
2. Aims of the study.	16
3. Material and methods:	17
3.1. Study subjects	17
3.2. Echocardiography	19
3.3. Strain rate measurements	20
3.4. Coronary angiography	23
3.5. Statistics	23
4. Summary of papers:	25
4.1. Paper 1 Real-time strain rate imaging	25
4.2. Paper 2 Strain rate imaging in regional dysfunction	26
4.3. Paper 3 Strain rate imaging in coronary diagnosis	27
4.4. Paper 4 Strain rate imaging in diastolic function	28
4.5. Paper 5 Strain rate propagation vs. flow propagation	29
5. Discussion.	30
5.1. Study subjects	30
5.2. Methods	31
5.2.1. <i>Validation</i>	31
5.2.2. <i>Applicability</i>	33
5.2.3. <i>M-mode measurements</i>	34
5.2.4. <i>Flow propagation measurements</i>	34
5.3. Findings	35
5.3.1. <i>The normal strain rate pattern</i>	35
5.3.2. <i>Systolic function</i>	36
5.3.3. <i>Diastolic function</i>	37
5.3.4. <i>Flow measurements</i>	40
5.4. Limitations of the studies	46
5.5. Advantages of the strain rate imaging method	46
5.6. Limitations of the strain rate imaging method	48
5.6.1. <i>Aliasing</i>	48
5.6.2. <i>Reverberations</i>	48
5.6.3. <i>Noise</i>	49
5.6.4. <i>Frame rate</i>	51
5.6.5. <i>Spatial resolution</i>	51
5.6.6. <i>Insonation angle</i>	51
5.6.7. <i>One-dimensional measurement</i>	53
5.6.8. <i>Strain is wall deformation</i>	54
5.7. Strain rate or Strain?	54
5.8. SRI vs. DTI	55
5.9. Potential of SRI and possible future developments	56
6. Conclusions.	57
7. References.	58
Appendix: Mathematics of strain and strain rate.	64

Acknowledgements:

The present work was carried out at the Section of Cardiology, department of medicine, University Hospital of Trondheim, in the years 1996 to 1999. The Norwegian Council for Cardiovascular diseases, where I was employed as a research fellow during the period, financed the work.

My principal gratitude is toward my supervisor, Professor Terje Skjærpe, who suggested the idea of my entering the field of research in the first place, and the original line of investigation. During the research period, he has let me follow my own ideas, and at the same time being accessible with support and ideas. In addition, he has assisted in doing repeated measurements, and being constantly helpful in preparing all papers.

Andreas Heimdal, in the department of Physiology and Biomedical engineering, University of Trondheim with his co-workers, was the original inventor of the method of strain rate imaging. Andreas was in the beginning interested in strain measurement, firstly by speckle tracking, later by tissue Doppler. At the same time I was lucky in being already engaged in research in the longitudinal function of the left ventricle. This lucky coincidence led to discussions resulting in the application of longitudinal measurements, making real-time Strain Rate Imaging feasible. (For reasons discussed later, the SRI method is less feasible for transverse measurements, which had hitherto been the approach to velocity gradients.) The subsequent research in the feasibility, validation and physiology changed the course of my project as well, and made the period extremely rewarding as well as exciting. Fig. 2 and fig. 6 in this dissertation are modifications of a figures I have loaned from Andreas.

I also wish to thank his colleagues at the institute. Stein Inge Rabben, with whom I have collaborated in related work, has taught me a lot about the theoretical background of left ventricular mechanics. Sevald Berg has been working with Andreas in implementing the real-time application and off-line analysis of SRI. Hans Torp, the supervisor of Andreas has supplied inspiration as well as ideas, and knowledge. Bjørn Angelsen has likewise been present in the institute as an inspirator.

My colleagues in the section of cardiology, Knut Bjørnstad and Stig Slørdahl have been constantly supportive, as well as being important co-workers in assessing the precision of measurements.

Rune Wiseth, Morten Slette and Harald Vik-Mo did the coronary angiography examinations in paper 3. Without those, strain rate imaging would have no external reference for validation, as well as the important interpretations leading to the findings in paper 4 and 5.

In entering research rather late in my career, I feel that I have benefited to a great degree by clinical experience, which I believe have influenced my approaches to research as well. I owe much of my training in clinical internal medicine to my years as a resident in the department

of internal medicine, Namdal Hospital, an especially to the department chief, Ole Dehli, who was an exceptionally gifted clinician. He was also the first to show me the beginnings of echocardiography, and initiating my interest in cardiology.

The section of Cardiology, department of Internal medicine of the University Hospital of Trondheim, where I have worked as both junior and senior resident, as well as consultant, have been as important in training. All my senior colleagues have been important for education. I have, however, had the great luck to be employed during the tenure of Liv Hatle, who has taught me much about echocardiography, as well as being a great inspiration.

Although she had left the hospital when I started research, she has been continuously interested and encouraging when we have met.

Our Study nurses, Torild Vigeland Nergaard and Marit Olstad Røe have been invaluable in managing and assisting in the patient studies.

In paper 1, T. Bakke and T. Urdalen implemented the real-time algorithm, A. V. Lund, B. Olstad and S. Berg implemented the post processing software. Bjørn Olstad developed the software for analysis of colour Doppler data, and have been developing the application to meet the demands of the new techniques. Lars Åke Brodin and Bjørn Olstad invented the curved M-mode used in some of the papers.

And finally my wife Lise, for always being patient as well as supportive, and especially for always being there.

List of Papers:

- Heimdal A, Stoylen A, Torp H, Skjaerpe T. Real-time strain rate imaging of the left ventricle by ultrasound. *J Am Soc Echocardiogr* 1998;11:1013-19
- Stoylen A, Heimdal A, Bjornstad K, Torp H, Skjaerpe T. Strain rate imaging by ultrasound in the diagnosis of regional dysfunction of the left ventricle. *Echocardiography* 1999; 16, (4): 321-9
- Stoylen A, Heimdal A, Bjornstad K, Wiseth R, Vik-Mo H, Torp H, Angelsen B, Skjærpe T. Strain rate imaging by ultrasound in the diagnosis of coronary artery disease. *J Am Soc Echocardiogr* 2000;13(12):1053-64
- Stoylen A, Slordahl S, Skjelvan GK, Heimdal A, Skjaerpe T. Strain Rate Imaging in Normal and Reduced Diastolic Function: Comparison with Pulsed Doppler Tissue Imaging of the Mitral Annulus. *J Am Soc Echocardiogr* 2001 Apr;14(4):264-74.
- Stoylen A, Skjelvan G, Skjaerpe T. Inverse relation between strain rate propagation velocity and flow propagation velocity during early diastolic filling phase. Comparison between colour Strain Rate Imaging and colour M-mode. (Submitted).

Abbreviations and definitions:

A:	Atrial filling phase – atrial systole
E:	Early filling phase – early (ventricular) relaxation
AVPD:	Atrio ventricular plane descent (= MAE)
DTI:	Doppler Tissue Imaging – Tissue Doppler
cDTI:	Colour Tissue Doppler
pw DTI:	pulsed Wave Tissue Doppler
Dec-T:	Deceleration time of early mitral flow
ϵ :	Lagrangian strain (Mathematical)
E :	" (Mathematical)
LS:	" (Acronym)
ϵ' :	Natural strain (Mathematical)
E' :	" (Mathematical)
NS:	" (Acronym)
$\dot{\epsilon}$ and $\dot{\epsilon}'$:	Strain rate (Mathematical)
SR:	" (Acronym)
To differentiate, SR can be used as the name for the strain rate estimator.	
Ef:	Ejection fraction = $\frac{LVEDV - LVESV}{LVESV}$
IVR:	Isovolumic relaxation time
LVEDV:	Left Ventricular End Diastolic Volume
LVESV:	Left Ventricular End Systolic Volume
MAE:	Mitral annulus excursion (total motion of the base of the heart)
PSSR:	Peak systolic strain rate
PSR _s :	Peak systolic strain rate
PSR _e :	Peak strain rate of early filling
PSR _a :	Peak strain rate of atrial systole
PVF _e :	Propagation velocity of flow in early diastole
PVS _e :	Propagation velocity of strain rate in early diastole
SRI:	Strain rate Imaging
VG:	Velocity gradient
W:	Wall thickness (instantaneous)
W _d	Diastolic wall thickness
W _s	Systolic wall thickness.
WMS:	Wall Motion Score
WMSI:	Wall motion Score Index = $\frac{\Sigma WMS}{\text{Number of evaluated segments}}$

1. Introduction:

1.1. The concept of strain.

Strain, in daily language means, “stretching”. In scientific usage, the definition is extended to mean “deformation”. The concept of strain is complex, but linear strain can be defined by the Lagrangian formula:

$$1) \quad \varepsilon = \frac{L - L_0}{L_0} = \frac{\Delta L}{L_0}$$

Where ε is strain, L_0 = baseline length and L is the instantaneous length at the time of measurement. Thus strain is deformation of an object, relative to its original length. By this definition, strain is a dimensionless ratio, and is often expressed in percent. By definition, positive strain is lengthening or stretching, in accordance with the everyday usage of the term, negative strain is shortening or compression. The Lagrangian formula does only describe strain in one dimension as shown in fig. 1a). In two dimensions, strain has four components, two normal strains and two shear strains as shown in Fig. 1b). In three dimensions, there are nine components, three normal and six shear strains.

In an incompressible object, however, it is important to realise that the different strain components are simultaneous. In general, strain has to be balanced by inverse strain in one or more normal directions, due to the conservation of volume (not mass), as illustrated in fig 2. Incompressibility means that the mass conserves its volume, i.e. the volume is constant, and the sum of strain in three directions will be zero under the assumption that there is no shear strain. (This may serve as a definition of incompressibility):

$$2) \quad \varepsilon_x + \varepsilon_y + \varepsilon_z = 0$$

Mirsky and Parmley (1) originally introduced the concept of myocardial strain, to describe myocardial deformation. Traditionally, the three directions of the heart have been defined as transmural (radial), longitudinal (meridional) and circumferential, for instance in the description of wall stress (2), instead of the right-angled Cartesian coordinate system. This is illustrated in Fig. 3. In relation to the ultrasound plane of 2D echocardiography, still another set of directions can be defined: axial (or radial!), transverse (or lateral!) and elevation (out of plane) (3).

In M-mode echocardiography, wall thickening is a measure of contraction. Wall thickening is the relative increase in thickness during systole, defined as:

$$3) \quad \text{WT} = \frac{W_d - W_s}{W_d} = \frac{\Delta W}{W_d},$$

in other words the transmural strain of the wall. From this formula, it follows that transmural strain is positive during systole, negative during diastole.

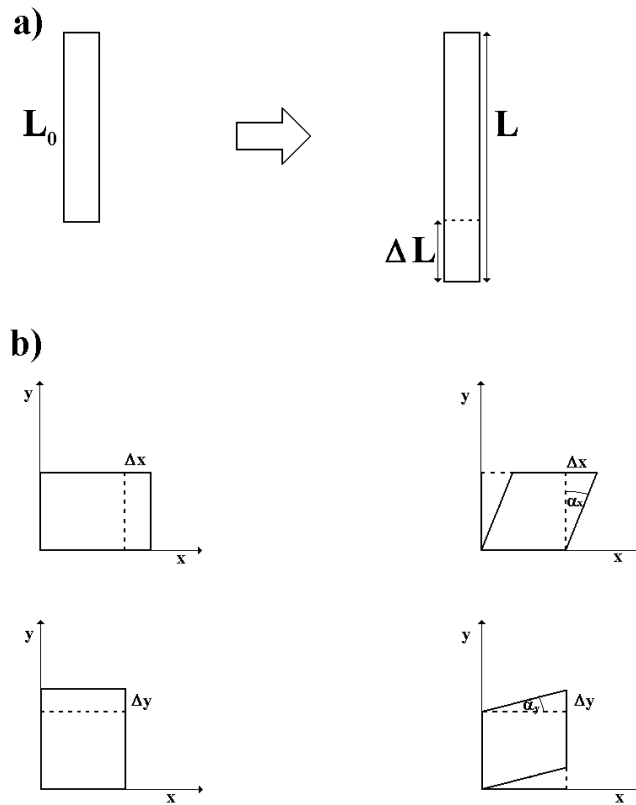


Fig. 1. Deformation of an object.

- a)** One-dimensional deformation. Strain is deformation relative to its original length,

$$\epsilon = \frac{L-L_0}{L_0} = \frac{\Delta L}{L_0}, \text{ the figure shows positive strain (lengthening).}$$

- b)** Two-dimensional deformation. Deformation in two dimensions can be described by four components: Two normal strains (normal or perpendicular to the surface), lengthening and shortening along the x and y axis: $\epsilon_x = \frac{\Delta x}{x}$ and $\epsilon_y = \frac{\Delta y}{y}$, and two shear strains, characterised by the displacement of one border relative to the other:

$$\epsilon_{xy} = \frac{\Delta x}{y} \text{ and } \epsilon_{yx} = \frac{\Delta y}{x} \text{ or angles of deformation, } \alpha_x \text{ and } \alpha_y, \text{ where it is obvious from the figure that } \epsilon_{xy} = \tan(\alpha_x) \text{ and } \epsilon_{yx} = \tan(\alpha_y).$$

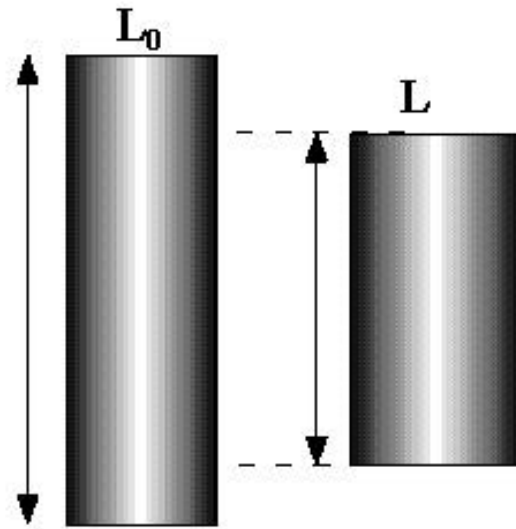


Fig. 2. Strain in three dimensions. The cylinder shows strain, which can be described as Lagrangian strain from L_0 to L . However, the figure also shows simultaneous thickening or expansion in the two transverse directions. If the cylinder is incompressible, the sum of the longitudinal and the two transverse strains will be zero; $\epsilon_x + \epsilon_y + \epsilon_z = 0$, and the volume remains constant.

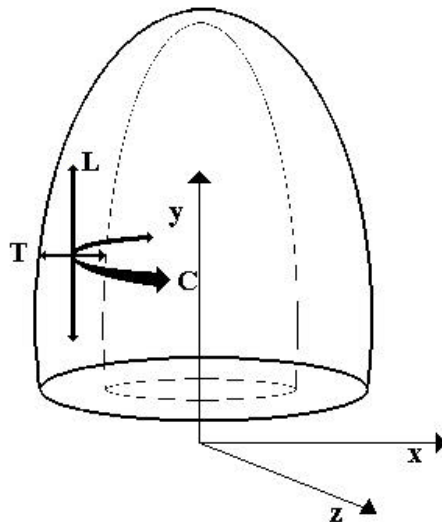


Fig. 3. The three main directions of the left ventricle: Longitudinal or meridional (L), transverse / transmural or radial (T) and circumferential (C). The term “transmural” should probably be preferred, as radial has another interpretation when applied to the ultrasound beam, and transverse when applied to the 2D-picture. The circumferential axis is local, perpendicular to the two others, and tangential to the wall in each point. The axes are compared to the Cartesian coordinate system of x , y and z .

1.2. Longitudinal motion of the heart

It has previously been shown that the base of the heart descends toward the apex during systole (4, 5, 6, 7, 8, 9, 10). The apex remains virtually stationary throughout the heart cycle moving a few millimetres in the same direction as the base (6), as known from the clinical experience of the apex beat as a systolic event, and demonstrated by apexcardiography and echocardiography. The descent of the base is 1.2 – 1.5 cm in healthy subjects (4, 7, 8, 9) and both the magnitude of the motion and the peak velocity is correlated to ejection fraction (7, 8, 9,10) and thus also to prognosis after myocardial infarction (11). During the diastolic phases of early filling (E) and atrial systole (A), the base of the heart returns to the original position (12, 13, 14). The descent of the base (mitral annulus excursion or MAE), is a measure of the systolic shortening of the ventricle. Shortening of the ventricle is measured in absolute values, but the relative change in length is the longitudinal strain. Longitudinal strain is thus negative during systole and positive during diastole.

Thus the relation between longitudinal and transmural strain is inverse, in the same manner as illustrated in fig. 4, i.e. as the ventricle shortens, the wall thickens, as the ventricle elongates, the wall thins. As well as being an empirical fact, demonstrated by echocardiography, it also follows from the incompressibility of muscle.

The relation to circumferential strain is not well established. As the chamber dilates during diastole, and narrows during systole, the circumferential strain has to be negative during systole, positive during diastole. But as the outer contour of the left ventricle is relatively unchanged during the heart cycle (4), depending on where the strain is measured (epicardial, midwall or endocardial), the circumferential strain can be near zero during the whole heart cycle, chamber dilation being mainly a function of wall thinning. In that case, the main strains of the ventricle are the longitudinal and transverse. The circumferential fibre function will then mainly be the balancing of the internal pressure (4). In addition, MR has demonstrated shear strain in the form of systolic “twisting” and diastolic “untwisting”, i.e. torsion of the whole heart (15). MR can measure all strain components simultaneously, and may be the reference method.

And finally, as the fibre architecture of the heart is complex, as well as rearranging during the heart cycle, the relation to actual fibre strain is even more complex.

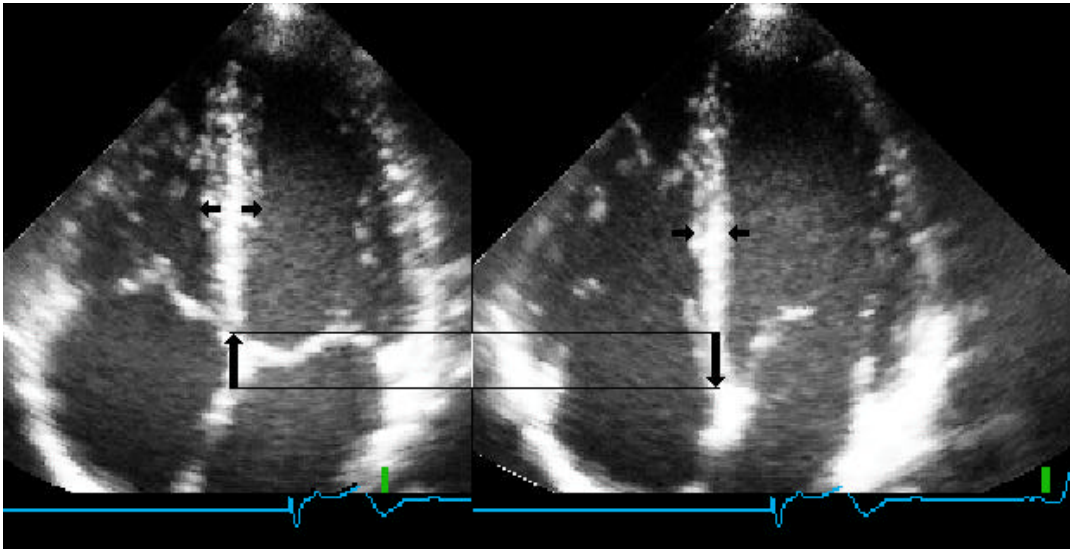


Fig. 4 Illustration of the incompressibility of the myocardium. As the wall stretches in diastole, it thins, as it shortens in systole, it thickens, showing the inverse relation of longitudinal and transverse strain.

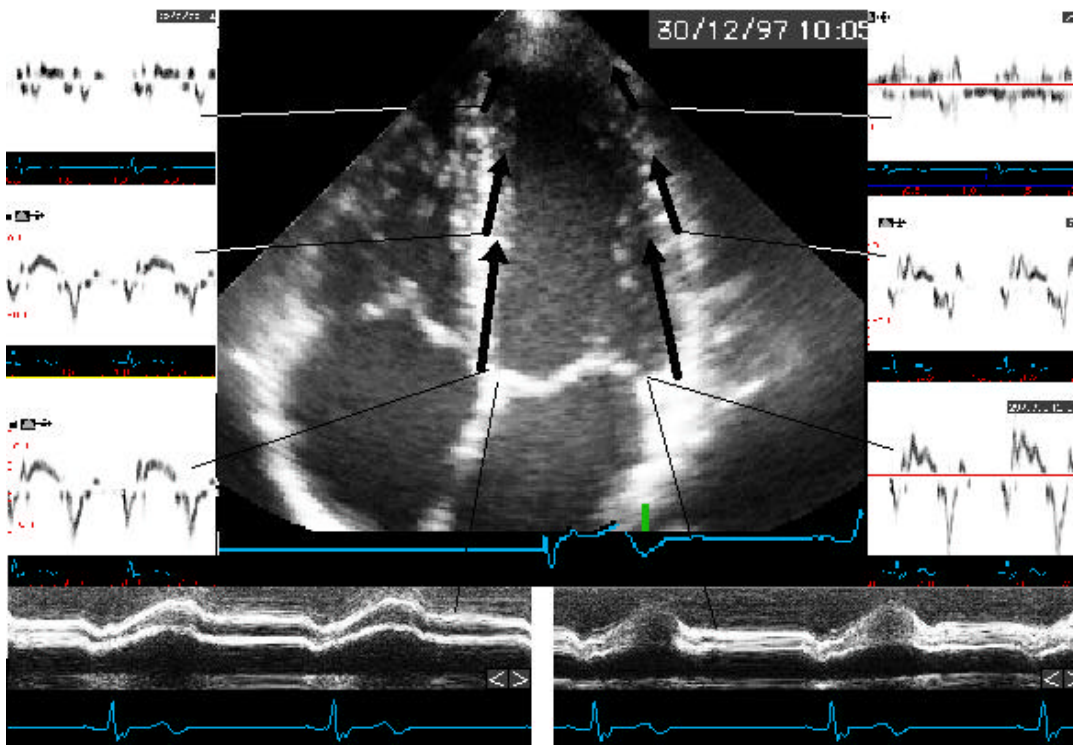


Fig. 5. The differential velocities of the left ventricle. While the apex is stationary, the annular plane moves as indicated by the longitudinal M-mode curves below the 4-chamber picture. The decreasing systolic velocities at the different levels is illustrated by the arrows, and by the same time shown by the pulsed tissue Doppler curves to the sides. Thus the ventricle has longitudinal velocity gradients.

1.3 Strain rate

The strain rate is the instantaneous strain (or change in strain) per time unit.

$$4) \quad \dot{\epsilon} = \frac{\Delta\epsilon}{\Delta t}$$

The unit of strain rate is cm/s/cm, or s⁻¹. The strain rate has the same direction as the strain, i.e. negative strain rate during shortening, positive strain during elongation.

1.4. The velocity gradient

The concept of velocity gradient was introduced by Fleming et al (16). The velocity gradient is defined as the slope of the linear regression of the myocardial velocities along the M-mode line across the myocardial wall. This is equal to the difference in endocardial and epicardial velocities, divided by the instantaneous wall thickness (W).

$$5) \quad VG = \frac{V_{\text{endo}} - V_{\text{epi}}}{W} = \frac{\Delta v}{W}$$

The definition was extended by Uematsu et al (17) to include the transmural velocity gradient across the parts of the wall where the scanline is not perpendicular to the wall, by the cosine correction of the velocities. The velocity gradient measured in this way, was transmural or radial.

As transmural strain rate is the rate of change in wall thickness, the strain rate is the

$$6) \quad \dot{\epsilon} = \frac{\Delta W/W_d}{\Delta t} \approx \frac{\Delta W/\Delta t}{W} = \frac{\Delta v}{W}$$

In other words, the velocity gradient is an estimator of the transmural strain rate, strain per time unit approximates velocity per length unit. (The reason this is an approximation, is that W is the instantaneous thickness, corresponding to L in formula 1), while L₀ is constant, corresponding to f.i. W_d. This is discussed in more detail in appendix A.)

As the moving base descends toward the stationary apex, the tissue velocities have to increase from the apex to the base (fig. 5). This has also been established previously (18). During diastole, and especially the two main filling phases of early filling, (E) and atrial systole (A), the base reverts to its original position (12, 13, 14). The diastolic velocities decrease from the base to the apex as well, and the ventricle thus has longitudinal velocity gradients.

The definition of the velocity gradient can thus be generalised further:

$$7) \quad VG = \frac{(v_2 - v_1)}{r} = \frac{\Delta v}{r},$$

where r is the distance between the points of velocity measurements. In this definition, it can be applied to longitudinal as well as transmural strain.

1.5 Strain rate Imaging by Ultrasound

The longitudinal velocities of the myocardium can be sampled simultaneously in all points of a plane during the heart cycle by colour Doppler Tissue Imaging (DTI) from the apical view. In colour Doppler, the simultaneous velocities are stored as colour coding, but the actual values can be extracted off-line (18).

The algorithm in 7) is simple enough to be implemented in real-time processing or post-processing of tissue colour Doppler. (In fact, this is an approximation, in reality both velocities and strain rates are measured by autocorrelation of the phase shift). The method is termed Strain Rate Imaging (SRI) (19) and estimates strain rate by the velocity gradients:

$$8) \quad \text{SR} = \frac{v(x) - v(x + \Delta x)}{\Delta x} = \frac{\Delta v}{\Delta x} = \frac{(v_2 - v_1)}{r} = \text{VG} \approx \dot{\epsilon},$$

as shown in Fig. 6.

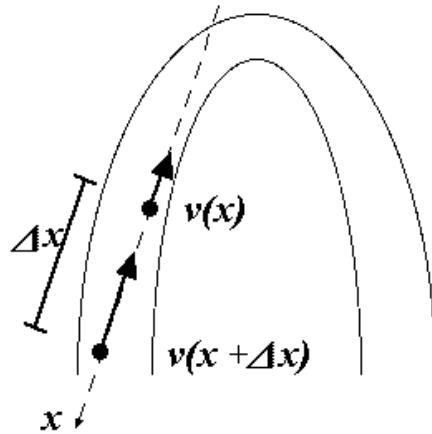
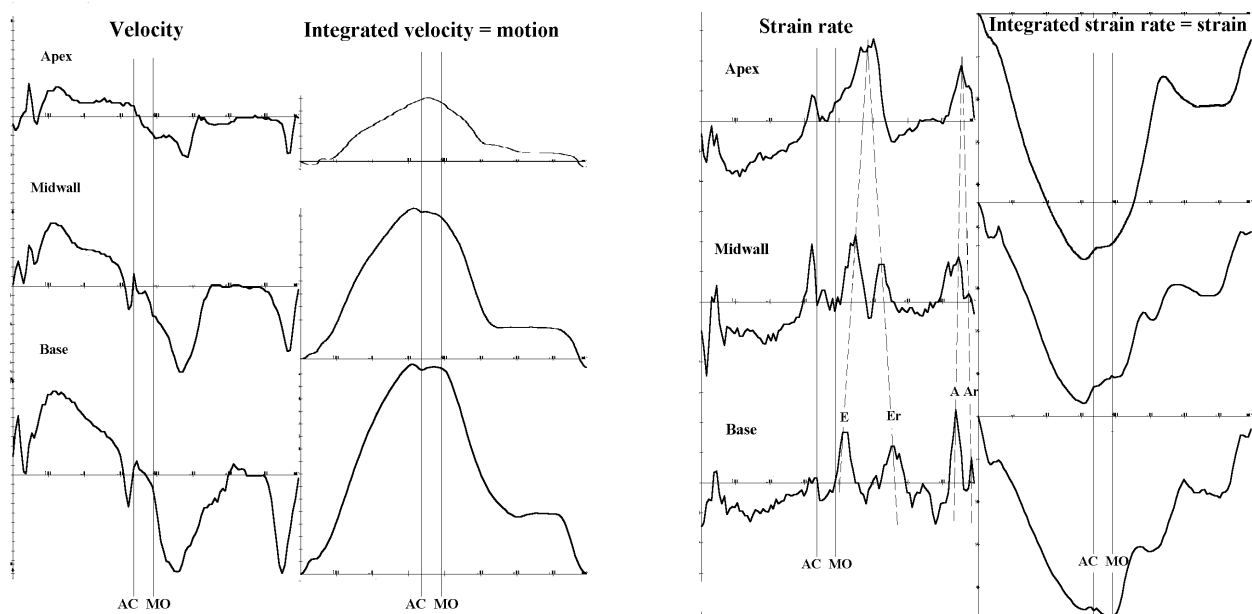


Fig. 6. The figure illustrates the longitudinal strain rate estimation by the velocities of two points of the myocardium with the distance Δx . The offset distance is exaggerated for clarity. The points of velocity measurements are points in space, not in the myocardium, as illustrated in this picture, where v_2 is measured at the point x , i.e. $v(x)$, while v_1 is measured along the same line, at a point $v(x + \Delta x)$ i.e. at the distance Δx from x . This means that as the muscle segment along Δx shortens, in the next frame there will be a new muscle segment with the unchanged length Δx , and the estimator $\text{SR} = \frac{v(x) - v(x + \Delta x)}{\Delta x}$ is not the same as the velocity gradient as originally defined. It can be shown, however, that the ratio is exactly equal to the velocity gradient. (Appendix A).

Analogous to colour Doppler, the resulting strain rate values / velocity gradients can be colour mapped or extracted as numerical values and curves. The temporal resolution of the post-processed M-mode is equal to the frame rate in 2D recording, up to 130 FPS when acquiring colour DTI images of the whole left ventricle. As the intention is to visualise presence and magnitude as well as direction of wall deformation, we have chosen a three-colour map, where cyan to blue colours are positive strain rate, and yellow to red are negative strain rate. Green represents periods and areas of no strain, i.e. below the low rate reject limit. The colour map is reproduced at its best in paper 3, fig. 4, while strain rate and strain curves are shown in Fig. 7.



a)

b)

Fig 7.

- a) Velocity data from septum of a normal ventricle. The velocity curves to the left are from the base, midwall and apical levels. To the right of each velocity curve are post-processed integral curves of the velocity, showing the motion of the same points. Characteristic of velocity and motion curves are the reduction of amplitude from the base to the apex (18). AC: aortic closure. MO: mitral opening.
- b) Strain rate data. The curves are post processed strain rate from the velocity data of fig. 18a), i.e. the same data set, from the basal, midwall and apical level of the septum. The strain rate curves shows the local rate of deformation. To the left of each curve is shown the integral curve, showing the strain, or local deformation of the same length. Characteristic of strain rate curves is the constant amplitude of all phases, showing that the velocity decreases evenly from base to apex. AC: aortic closure. The closure is at the end of the positive spike representing the protodiastolic lengthening (43). MO: Mitral opening. E: Elongation during early filling. A: Elongation during atrial systole. It is more evident than from velocity data that the E- and A- phases are delayed at the apex relative to the base, propagating along the wall. Finally is seen the positive spikes of the return of the waves, Er and Ar, probably due to the waves from the opposite wall.

For technical reasons, the method is best suited to studies of the longitudinal strain rate. Firstly, the noise sensitivity (noise to signal ratio) increases as the offset distance Δx between the points of velocity measurements decrease, giving a practical lower limit of spatial resolution of SRI of about 5 – 10 mm. Secondly, the points of measurement remains fixed in space, giving false measurements if the myocardium moves in and out of the sample length, which is more likely to happen in the transverse measurement. The background for this is discussed in detail in 5.6.3 and 5.6.5, but the whole study is limited to longitudinal measurements.

The systolic velocity in any point in the myocardium is the resultant of the rate of shortening (longitudinal strain rate) from that point to the apex. The strain rate curve is similar to an inverted velocity curve as shown in comparing Fig. 7a and b. In SRI, the algorithm subtracts the velocity apical to the segment measured, i.e. the influence of the shortening of the more apical segments, so SRI measures the local shortening. In addition, this method will subtract velocities due to translation of the whole heart. Thus quantitative SRI will give measurement of local deformation rates and their time curves during the heart cycle. On the other hand, colour mapping gives semi-quantitative information of local strain rates, as well as quantitative information about the spatial-temporal relations between events in the ventricle during the heart cycle.

By summing the strain rate values of all frames times the sampling interval from each frame, the strain value in each pixel can be estimated:

$$9) \quad \Sigma(\text{SR} * \Delta t) = \Sigma\left(\frac{\Delta \epsilon}{\Delta t} * \Delta t\right) = \Sigma \Delta \epsilon = \epsilon$$

The integrated strain curve is shown in Fig. 7. Analogous to myocardial velocity and strain, the motion of a point can be seen as the resultant of the strain of all segments from the apex, and the strain curve is similar to an inverted motion curve integrated from velocity data or an M-mode curve of the annulus.

Early model experiments did show a good agreement between the measured strain rate by this method and the strain rate generated by the model (20).

Aims of the study:

General aim of this thesis

The main hypothesis is that strain rate imaging measures the local deformation of the ventricular wall, by the arguments above. The partial aims of each study are:

Specific aims of the studies

- c) To demonstrate that the method of Strain Rate Imaging is feasible in a clinical setting, and to evaluate whether the method could document differences between normal and pathological regional function in a pilot study.
- d) To compare regional wall function assessed by SRI with regional wall motion assessed by 2D-echocardiography in a patient group with reduced regional function (myocardial infarction). A reasonable correspondence between the two methods will constitute validation of findings by SRI as regional wall function assessment in a clinical setting.
- e)
 - a) To compare wall motion by SRI and by 2D echo against an external reference (coronary angiography) to compare sensitivity and specificity of each method as well as of the two methods combined for the detection of significant changes in regional wall function.
 - b) As wall motion scoring by 2D is wall thickening, and Strain Rate Imaging is wall shortening, to compare the information from the two methods.
 - c) To assess the precision of quantitative Strain Rate measurement against an external reference.
- f) To study the strain rate of the early filling phase, to compare with tissue Doppler data of the same phase and to study the difference between normal subjects and patients with delayed relaxation.
- g) The filling phases seen with colour strain rate reveals that wall stretching propagates from the base to the apex in a manner similar to flow propagation. The aim of the study in paper 5 is to compare the propagation of strain rate with the propagation of flow, over a wide range of values, both in normal subjects and in patients with delayed relaxation.

3. Material and methods:

3.1 Study subjects:

The normal subjects group consists of persons without any evidence of heart disease and with normal echocardiographic findings. In general the normal subjects were colleagues and staff at the hospital and at the institute of physiology and biomedical engineering. All were professionally acquainted with the procedure of echocardiography and gave informed consent to the examination. Files were anonymised.

The patients belonged to two different groups. The infarction patients for the validation and study of regional systolic function all had their first myocardial infarction, and were examined during their first hospital stay, in general during the first week. The examination was a normal, scheduled echocardiography examination for routine clinical indications. A clinical echocardiography report was given back to the ward as normal procedure. The recorded echocardiography files were then transmitted to a computer, and stored on CD for off-line analysis. Additional strain rate and tissue Doppler cine-loops were obtained during the examination, prolonging the examination by 3 to 5 minutes. Informed consent for the use of examination data for research purposes was obtained from all patients. The patients included in the study of SRI versus coronary angiography were included because angiography was decided for clinical indications. Inclusion and echocardiography was performed after angiography was decided. Of the patients in paper 2, five had a coronary angiography during hospital stay. They were included in the study in paper 3 as well, the subsequent 15 patients in paper 3 were new. No patients had coronary angiography for study purposes alone. The patient characteristics of the patients in paper 3 are summarised in table 1.

The hypertension patients, for the study of diastolic function were recruited from the LIFE echo substudy (21). The national ethical committee approved this study. The patients were recruited in a primary centre on the basis of hypertension plus criteria for left ventricular hypertrophy on the ECG, and entered a treatment schedule comparing losartan and atenolol in a randomised, blinded design, with additional antihypertensive treatment administered as needed. All medical treatment was administered at the primary centre. The patients in the echocardiography substudy were referred from the primary centre. The substudy consisted of yearly visits during five years, echocardiography done at each visit, recorded on video and sent to the core laboratory (Cornell University). The data obtained for the studies in paper 4 and 5 were all recorded during their visits after one to two years of treatment. The patients then had normal blood pressure on treatment, normal ejection fraction, minimal hypertrophy and moderately prolonged deceleration time and isovolumic relaxation time, indicative of delayed relaxation (22). The echocardiographer was blinded to all treatment. The patient

characteristics of the hypertension patients and normal subjects in paper 4 are summarised in table 2. As the study in paper 4 progressed, it became evident that the strain rate had a propagation pattern and normal values similar to that previously reported for flow propagation (23). The relation between these became an object of interest. The flow propagation data for study 5 were obtained during the second part of the first study. The subjects in the study in paper 5 are the 25 last (12 controls and 13 patients) of those in the study in paper 4, but the inclusion was done consecutively, without bias once the registration of colour flow was started. The strain rate measurements are the same data as in paper 4. The differences in diastolic function between controls and patients remained significant, although the numbers were reduced by the selection (table 3).

It is important that in all studies, once inclusion was decided, no study subjects were excluded for poor echo quality. The study population will therefore resemble a normal patient population in clinical practice where quality of echo data is concerned, and the precision given is clinically relevant.

Table 1: Patient characteristics of infarction patients (16 m., 4 f.) of paper 3:

	Age (years)	Peak ASAT (ECG: 12 ant. 8 inf.):	EF % (Simpson)	AMI age (days) at echo	AMI age (days) at echo
Median:	56	406	41	4	5
Maximum:	77	1419	54	30	29
Minimum:	37	100	22	1	0

EF: Ejection fraction. AMI: myocardial infarction.

Table 2: Subject characteristics in the study in paper 4. Group averages with standard deviations in parentheses and P values for differences:

	Age (years)	EF %	HR	BP mmHg	IVSd mm	LVD mm	Dec-t ms	IVR ms	MVE cm/s	MVA cm/s
Controls	40 (14)	56 (6)	63 (11)	125/77 (14/14)	8 (1)	57 (5)	183 (32)	77 (15)	74 (13)	53 (14)
Patients	65 (6)	55 (6)	61 (14)	153/85 (18/6)	10 (2)	53 (11)	252 (48)	103 (19)	70 (20)	74 (19)
P:	<0.001	NS	NS	<0.01	<0.001	NS	<0.001	<0.001	NS	<0.001

Table 3: Subject characteristics of the subgroup in paper 5.

	Age Years	HR	BP mmHg	EF %	IVSd mm	LVD mm	DTIe cm/s	Dec-t ms	IVR ms	E/A
Control	46	65	133/79	57	7	57	12.8	191	73	1.74
Patient	65	60	154/85	54	10	54	8.7	238	99	1.02
P:	<0.001	NS	<0.01	NS	<0.005	NS	<0.005	<0.005	<0.002	0.05

HR: heart rate. **BP:** blood pressure. **IVSd:** septum thickness in diastole. **LVDd:** left ventricular diameter in diastole. **DTIe:** peak early diastolic mitral annulus velocity by tissue Doppler. **Dec-t:** Deceleration time of mitral flow E-wave. **IVR:** Isovolumic relaxation. **MVE:** peak flow velocity of mitral E-wave. **MVA:** peak flow velocity of mitral A-wave. **E/A:** Ratio of the two.

3.2 Echocardiography:

All recordings in this study were obtained with a Vingmed System FiVe scanner with a 2.5 MHz phased array transducer. Ordinary echocardiography recordings of 2D cine-loops of five standard planes, transverse M-mode recordings, pulsed wave Doppler and colour Doppler flow as well as pulsed wave Tissue Doppler of the mitral ring were transferred to a Macintosh computer for off-line analysis in EchoPAC (GE Vingmed Ultrasound, Horten, Norway). All 2D and M-mode recordings were done in the second harmonic mode. Pulsed Doppler recordings of mitral inflow velocity curves were obtained with the sample volume between the tips of the mitral leaflets. Isovolumic relaxation time was measured with the sample volume between aortic and mitral annulus, so that the valve click of aortic closure as well as the start of mitral flow was seen. Pulsed tissue Doppler recordings of the mitral annulus velocities were obtained from four points of the mitral ring: Septal and lateral in the four-chamber plane and anterior and posterior in the two-chamber plane. Average values of peak systolic and peak early and late diastolic velocities were computed.

Both 2D, colour Doppler and Strain rate cine-loops were of the three standard apical planes (4-chamber, 2-chamber and long axis). Ejection fraction was measured by endocardial tracings from 4-chamber and long axis planes, and calculated by modified Simpson's method. In paper 2 and 3, wall motion was scored in a 4-level scale (Wall Motion Score, WMS):

1. Normal
2. Hypokinetic
3. Akinetic
4. Dyskinetic

in the standard 16 segment model of the left ventricle (24) illustrated in fig. 8.

Pathological finding (dyssynergy) was all levels above 1. Further levels of 5: Scar or 6: aneurysm was not used, as these are anatomical and not functional terms. Wall motion score index (WMSI) was calculated in the usual way (25), as the average wall motion score of the number (N) of evaluable segments ($WMSI = \frac{\sum WMS}{N}$).

An expert stress echocardiographer (Bjørnstad) who was blinded to patient data of infarct location assessed wall motion score in 2D recordings. Emphasis was placed on wall thickening, not endocardial excursion, to minimise the effects of tethering.

3.3 Strain rate measurements:

On-line strain rate recordings were obtained by special programming. During the pilot study in the first paper, the first recordings were obtained as RF-data, transferred and post-processed to colour tissue velocity as well as colour strain rate recordings. In the last four subjects of the first study, the online application was used. In the rest of the studies, online strain data was obtained by processing colour tissue Doppler data as described previously either by recording SRI cine-loops directly on the scanner, or by recording colour DTI and processing SRI data by off-line processing. The Strain Rate application was specially programmed on the scanner. The settings of the scanner were set to maximum lateral averaging, to minimise noise. This also means that strain rate would be averaged over the whole thickness of the wall, so lateral placement of M-mode lines or sample volumes were of little consequence. On the other hand, no comparisons of different levels across the wall were possible. The offset length (Δx) in the studies was 5-7 mm; making radial resolution equal to the offset plus the pulse length. The frame rate was around 70 with online SRI, and up to 132

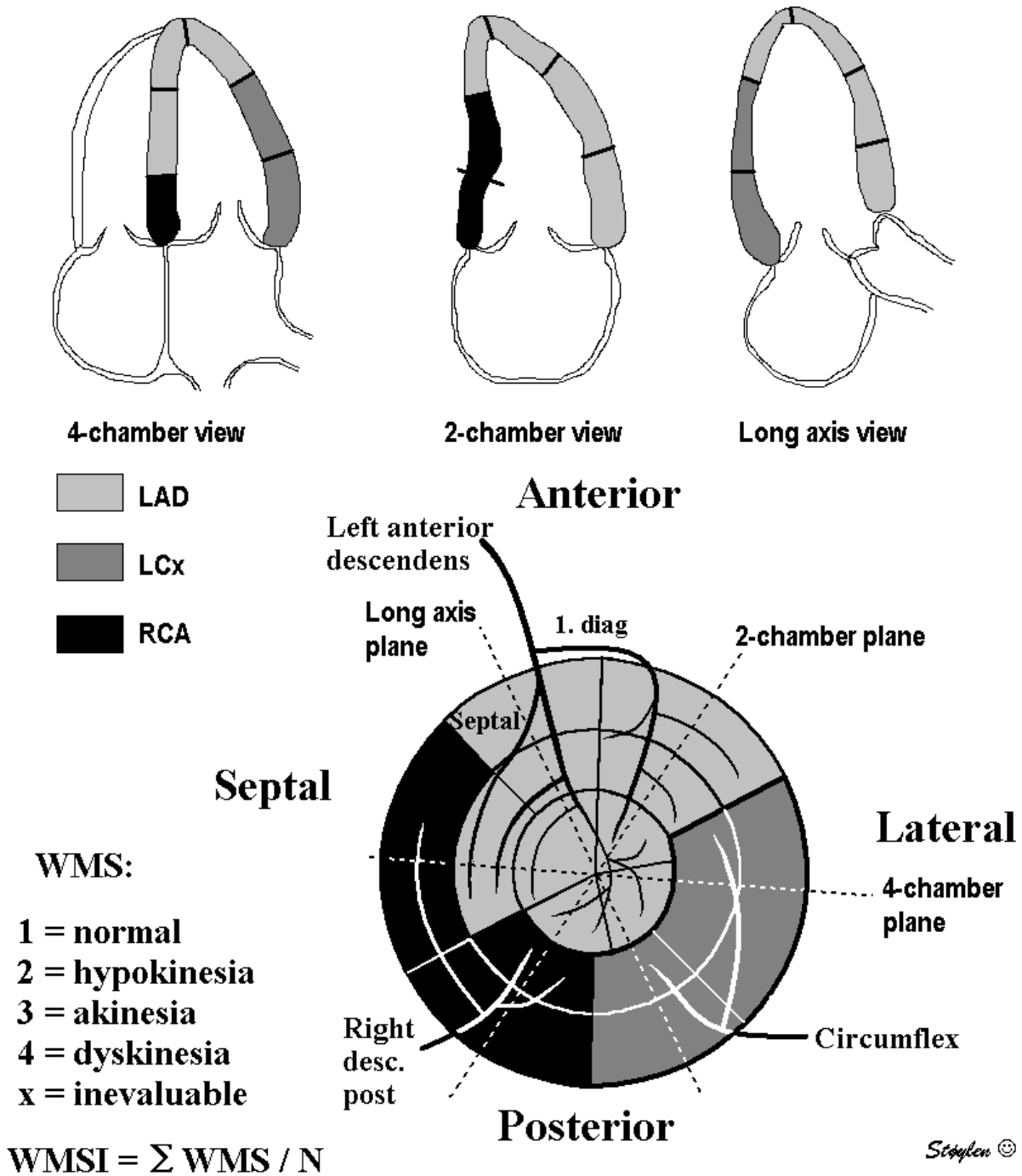


Fig. 8. The 16 segment model of the left ventricle (18). The relation to the different arterial beds is shown (19). The relation to the coronary anatomy is superimposed, making it possible to relate echocardiographic segments to coronary anatomy. The wall motion score (WMS), is the assessment of the four functional levels of wall function. Wall motion score index (WMSI) is the average WMS of all evaluable segments.

with DTI (and hence, off-line SRI). The high frame rate was due to the reduction in the number of tissue scanlines, as temporal resolution is considered the main objective in tissue Doppler. The difference in frame rate between strain rate and DTI was a matter of scanner presets in the experimental stage. At that point in time, it was uncertain whether additional tissue information or temporal resolution was most important. The theoretical limit for frame rate in online SRI is the same as for colour DTI, and scanner presets can be adjusted accordingly. The low strain reject limit was in all studies between ± 0.1 and 0.3 s^{-1} . Cine-loops were transferred to a PC computer and analysed in a dedicated software application, and colour cine-loops were analysed in the curved M-mode (26) with wall motion score, in papers 2 and 3. The actual acquisition of the three SRI loops, was a matter of less than one minute, the transfer to computer (by FTP) about the same, while the segmental analysis is time consuming, but comparable to segmental analysis of 2D cine-loops.

Colour SRI is semi-quantitative, as is wall motion assessment. That makes the two methods more directly comparable than proceeding directly to quantitative strain rate measurement. Wall shortening could then be graded as Wall Motion Score in a similar 4-level scale as wall thickening. The colour scale for WMS by SRI is reproduced in paper 3. Wall motion score by SRI was primarily assessed by me, unblinded to infarct location, but blinded to angiography findings in paper 3. Systolic wall function was scored by the four-level scale in all 16 segments in papers 2 and 3 and WMSI calculated in the same way as for 2D echo. Støylen and Skjærpe did the intra- and interobserver studies of colour SRI. Støylen had during the studies acquired the most experience with colour SRI, while Skjærpe had a very wide general experience with echocardiography. Støylen did repeated readings with an interval of 4 – 12 months. Skjærpe did the first five patients in paper 2 as learning, the last 10 as evaluation, twice in a short interval, but with scrambled order the second time. In paper three, the last 15 were available for interobserver study.

When findings by SRI had been validated against 2D echocardiography in papers 2 and 3, quantitative strain rate measurement became an object of interest in paper 3. In this study both semi-quantitative assessment (wall motion score) and quantitative measurement of peak strain rate was done in all 16 standard segments. No repeatability study of quantitative strain rate measurement was done, as the study did show a low precision in quantitative measurement, with considerable overlap between segments with different wall motion score and angiography status.

In paper 4 and 5, peak strain rates of systole, early and late relaxation are measured in all 16 segments. In paper 3, regional systolic strain rate is compared to wall motion and coronary angiography. In paper 4 and 5, global average of peak strain rates is computed.

Propagation of the stretch wave of early relaxation was measured in a straight line M-mode for reasons discussed in 5.2.3. The results, however, seem to indicate that the curved M-mode

would give the correct measurements, if a standardised way of tracing it could be implemented.

Flow propagation velocity is measured by straight line tracing of the front of the aliased velocity, in colour M-mode as discussed in paper 5. The M-mode line was placed in mid-ventricle.

3.4 Coronary angiography.

This was done in the routine angiography laboratory. Indications for coronary angiography were clinical; either to do rescue PTCA after failed thrombolysis (in four patients) or because of persistent unstable angina after myocardial infarction. The patients were included in the study in paper 3 because the angiography was decided. No angiography was performed for study reasons. In all cases standard technique was employed. Infarct related artery (IRA) with culprit lesion was localised by comparing the angiogram with the ECG at admittance.

Coronary artery stenosis was calculated by quantitative angiography. A diameter stenosis of 50 % or more was considered significant.

The bull's eye map in fig. 8 is used in paper 3 to establish a relation between coronary and echocardiographic anatomy in accordance with general convention (24, 25). This relation is used both ways. By analysis of echocardiographic and SRI images, the infarct related artery was identified (blinded to the angiogram), and compared with the angiographic diagnosis. In the reverse analysis, the culprit lesion by comparing with the bull's eye map, could predict which segments were affected by the lesion, i.e. those assumed to be partly infarcted. They are called angiography positive or at-risk segments, the rest angiography negative.

This prediction however, neither takes into account the salvage effect of reperfusion resulting in normally functioning segments within affected areas, nor the effects of collaterals or affected neighbouring segments due to variations in smaller artery branches. In this study, only 4 patients had TIMI 0-1 flow at the time of echocardiography, the rest had 2-3 (27) after thrombolysis or rescue PTCA. The main point, however, was to establish an external reference for the comparison of the two ultrasound methods.

3.5 Statistics.

Both parametric and non-parametric statistics are used.

Comparison as well as repeatability of ordinal wall motion score assessment are by kappa and weighted kappa statistics. By kappa statistics, a κ -value of: < 0.20 is considered poor, 0.21 to 0.40 fair, 0.41 – 0.60 moderate, 0.61 – 0.80 good (28).

Repeatability of quantitative measurements is by Bland Altman statistics (95% confidence interval = limits of agreement = average of difference repeated measurements \pm 2SD of differences between them) (29).

Significance of differences between groups is by two-tailed students T-test. All significant differences were also tested significant by Wilcoxon's two-sample rank sum test. In paper 3, significance of differences between groups of segments is by ANOVA analysis.

Correlations in papers 2 and 3 (where correlation between WMSI and EF is a relatively minor point) is by Pearson's R, in paper 5 where correlations are the main objective, both Pearson's and Spearman's coefficients are given.

In paper 5, univariate and multivariate linear regression is used.

4. Summary of papers

4.1. Paper 1: Real-time Strain Rate Imaging.

Method, feasibility and pilot study.

This study is the pilot study, to see if Strain Rate Imaging was feasible in a clinical setting, and to see if the method could identify walls with segments with reduced systolic function.

The theory behind strain rate measurements and the practical application, as well as some of the limitations of the method is discussed. Six patients with acute myocardial infarction, and six normal subjects without evidence of heart disease were studied. The first four in each group were studied by the off-line RF method, the last 2 with the real-time application. Wall motion in all infarcted walls was seen as either hypo- or akinetic by colour. In the normal subjects, a similar number of walls were analysed. No hypo- or akinesia was seen. The actual strain rate values were assessed by the colour legend, giving a normal systolic strain rate of about -1.3 s^{-1} . In this study, we concluded that Strain Rate Imaging was and that it seemed to be able to differentiate between normal and pathological wall function.

In this paper Andreas Heimdal defined the strain rate concept, the description of the strain rate imaging technique and the discussion on the technical limitations. He also made figures 1 and 2, and the general revision of the whole paper. Asbjørn Støylen performed the patient study, including the actual ultrasound examination as well as the evaluation of findings in relation to the clinical data. He also wrote the discussion on the clinical application of the technique and made figs. 3 and 4 from actual ultrasound recordings.

4.2. Paper 2: Strain Rate Imaging in regional dysfunction.

Validation against 2D echocardiography in myocardial infarction.

In this study, 15 patients with myocardial infarction were examined. Systolic wall motion score (WMS) by longitudinal colour SRI and by 2D echo was compared. Of a total of 236 segments, 235 segments were analyzable by 2D echo and 218 by SRI. Wall Motion Score Index (WMSI) is a global parameter for left ventricular function, calculated as the average of segmental function. WMSI is used in the assessment of infarction and coronary artery disease. Both the number of dyssynergic segments and the degree of dyssynergy will contribute to the reduction in global function, and as a result a negative correlation of WMSI to Ejection Fraction can be expected. Correlation of WMSI with EF by biplane Simpson's method was -0.84 (95% CI -0.78 to -0.88, $p < 0,01$) by 2D and -0.92 (95% CI -0.89 to -0.94, $p < 0,01$) by SRI. 114 segments had equal score by the two methods, 51 segments differed by one degree and 14 by two, kappa value 0.45 (95% CI: 0.33 - 0.56). Intra- and interobserver agreement was also studied. Observer A had a κ -coefficient of intraobserver agreement of 0.51 (95%CI 0.41 – 0.63). Observer B, had a κ – coefficient for intraobserver agreement of 0.61 (0.50 – 0.72). The interobserver agreement of A and B was $\kappa = 0.32$ (0.10 – 0.36), and between B and 2D echo was $\kappa = 0.24$ (0.20 – 0.45). In conclusion, the agreement between 2D echo and SRI was fair to good. The precision of agreement is in the same order of magnitude as the precision for repeated measurements. In conclusion of this study, SRI seems to evaluate regional wall function.

4.3. Paper 3: Strain Rate Imaging in coronary diagnosis.

Comparison to 2D echocardiography and validation against coronary angiography in an infarction population.

In this study, 20 patients with acute myocardial infarction who underwent coronary angiography for clinical reasons were examined with SRI and standard echocardiography. Wall motion was graded by colour SRI and separately by wall thickening as in the previous study. SRI and 2D agreed well. The κ -coefficient of correspondence between methods, is 0.52 (95% CI 0.41 – 0.64), weighted κ 0.64. The variation between methods is of the same order of magnitude as the variability within methods. The study confirms the finding in the previous study, that SRI shows regional wall function.

The correlation coefficient (Pearson's R) of WMSI from 2D echo with EF was -0.83 (95% CI = -0.77 – -0.88), and from SRI with EF -0.82 (95% CI = -0.76 – -0.87). Culprit lesion and, hence, infarct-related artery (IRA) was identified from angiograms combined with ECG on admission. Both methods identified IRA in 19 possible cases and had equal sensitivity and specificity for at-risk wall segments. Combining the information from both methods did not change the accuracy. This can be taken to mean that the one method does not convey any additional information, in other words semiquantitative assessment of wall thickening and wall shortening are equivalent.

Peak systolic strain rate is measured in all accessible segments. Differences between the different groups of segments, is highly significant ($p < 0.001$) by ANOVA analysis. The difference between angiography positive and negative segments is significant as well, $P < 0.001$. The correlation of mean Peak Systolic Strain Rate with EF was -0.80 (-0.73 – -0.86). In conclusion, the study does show the feasibility and correspondence of quantitative measurement of peak strain rate as measurement of regional function. The wide standard deviations, as well as the overlap between measurements in both wall motion score groups and angio groups, however, indicates that peak strain rate in this application does not have sufficient precision for clinical utility.

4.4. Paper 4: Strain Rate Imaging in diastolic function.

Previous experience with SRI had shown that the early and late filling phase consisted of a wave of positive strain (elongation or stretch wave), propagating from the base to the apex. That finding was actually dependent upon resolving the velocities into velocity gradients. In this paper 26 hypertensive patients from the LIFE study and 28 normal controls were studied. Patients did show a significant reduction of peak systolic (9.5 vs. 7.5 cm/s, $p < 0.001$) and peak early diastolic (13.1 vs. 8.2 cm/s, $p < 0.001$) tissue velocity of the mitral annulus compared to controls. This is in accordance with other findings (30, 31).

Peak systolic strain rate (1.40 vs. 1.15 s^{-1} , $p < 0.001$), early diastolic strain rate (2.22 vs. 1.46 s^{-1} , $p < 0.001$) and propagation velocity of early diastolic strain rate (60.0 vs. 31.6 cm/s, $p < 0.001$) were reduced in the patient group. As in paper 3, peak strain rate measurements did show a rather low precision with wide standard deviations.

The findings by SRI are consistent with the DTI findings. Reduction in annular peak tissue velocity is a resultant of both reduced peak strain rate, as well as loss of simultaneity due to the slower propagation. Dividing the patients by heart rate did not show any indication of drug-specific effects. Dividing the controls by age did show a tendency to reduced diastolic function with increasing age, but still significant differences between the patients and the oldest controls.

In conclusion, the study does show that the diastolic function of the myocardium can be further analysed by the components of peak strain rate and propagation velocity of strain rate, and in delayed relaxation, both are reduced.

4.5. Paper 5: Strain rate propagation vs. flow propagation.

As the study in paper 4 progressed, it became evident that the propagation velocity of strain rate was reduced in delayed relaxation, as has been reported previously for flow propagation. (32, 33). In addition, the normal value for strain rate propagation was close to some reported for flow propagation (23). The relation between the two measurements became an object of interest. During the last half of the study, colour M-mode was recorded, and flow propagation velocity was measured. The strain rate data in this study are thus the same as the last 25 of the previous study. 12 normal subjects and 13 patients were studied. Early diastolic strain rate propagation velocity was reduced in the patient group (66.6 vs. 29.6 cm/s, $p < 0.001$). Early flow propagation velocity was increased in the patient group (69.9 vs. 54.8 cm/s, $p < 0.002$). In accordance with this, there was a negative correlation (Pearson's $R = -0.57$, 95% CI: -0.15 – -0.75, $p < 0.005$, Spearman's $R = -0.54$, $p < 0.005$) between strain rate propagation and flow propagation velocity. There was also a negative correlation between strain rate propagation and deceleration time of the mitral flow E-wave (Pearson's $R = -0.51$, 95% CI -0.15 – -0.75, $p < 0.05$, Spearman's $R = -0.48$, $p < 0.05$). No significant relation is found between flow propagation velocity and peak annular early diastolic velocity, left ventricular diastolic diameter, peak early diastolic strain rate, deceleration time of early mitral flow, isovolumic relaxation, HR, EF or age, in either univariate or multivariate analysis. Strain rate propagation velocity is significant in both univariate ($p = 0.003$) and multivariate ($p < 0.001$) analysis. Peak mitral flow velocity is not significant in univariate analysis, only in multivariate ($p = 0.014$), showing interaction with strain rate propagation velocity. In support of this, there is a significant correlation between the ratio: peak early mitral flow velocity / strain rate propagation (MVmax/PVSe) and flow propagation velocity, PVFe. Pearson's $R: 0.67$, 95% CI 0.37 to 0.84, $p < 0.001$, Spearman's $R: 0.58$, $p < 0.002$.

The conclusion of this study is that flow propagation seems to have more determinants than relaxation alone. Interaction between strain rate propagation and flow velocity may be of importance. Flow propagation is not a simple index of diastolic function in delayed relaxation. Both strain rate propagation and flow propagation does show a very limited precision, indicating a limited clinical utility at its present level.

5. Discussion

5.1. Study subjects.

No patients or normal controls were excluded for poor echo quality. This means that the study population resembles that of everyday clinical practice, so the precision limits are the level of precision to be expected in a clinical setting. One reviewer expressed surprise over the relatively low κ -coefficients in paper 3, reproduced in table 4. The limited precision of all methods is probably due to this.

All patients in the study in paper 3 had an angiography during the in-hospital phase. Of these, 16 had TIMI flow 2-3 (27), indicating reperfusion in the acute stage, while 4 had grade 0-1, and had a PTCA in relation to the angiography. (Also patients with grade 2-3 had PTCA in many instances, but this was to improve stenosis, not for salvaging myocardium.) Only two patients were examined by echo before very early PTCA, and both of these had TIMI grade 2-3. In reality, this means that all patients had reperfusion. This has probably resulted in a certain percentage of salvaged myocardium with normal function in some at-risk-segments by angiography. This will give an apparent reduction in the sensitivity of echocardiography and SRI for at-risk segments. It will not, however affect the comparison of the two methods.

In the studies in paper 4 and 5, there is a significant difference in age between patients and controls. As diastolic Tissue Doppler measurements are age-dependent (30), SRI data should be as well. Thus, some of the differences may be due to age. The separation of the control group into age intervals does show this, strain rate and strain rate propagation are all reduced with increasing age. The differences between the oldest controls and the patients are still significant, though. The main point however, of this study, is the study of the strain rate of diastolic function per se, regardless of causes. The age differences, although hardly significant due to the small groups, tend to support the main findings, that in decreased diastolic function, both strain rate and strain rate propagation during early filling is reduced.

The patients in paper 4 and 5 were on treatment during the examinations. The medication may have influenced the findings. As half of them were on losartan, the other half on atenolol, segregating them by heart rate as was done in paper 4, should increase the proportion of β -blocker treatment in the low heart rate group, and losartan in the high heart rate group. Any drug-specific effects would presumably have shown up as differences between those groups. None did, however, indicating that the findings are more probably related to diastolic function than to medication. One significant difference, the increase in peak strain rate during atrial systole, can be attributed to longer diastole rather than drug effects (other than on heart rate). Considering the number of measurements examined, the difference may even not be

significant. Applying Bonferoni's correction of the p value for the number of variables, it is not. The main differences in annulus velocities, peak early diastolic strain rate and propagation velocity, remains significant event with this.

Studies in isolated heart muscle (34, 35) have shown the velocity of contraction / relaxation to be load-dependent. Examining patients on treatment, with normalised blood pressure, supposedly would normalise the afterload, and reduce the impact of blood pressure. This would make the study "cleaner" regarding delayed relaxation per se. Tissue velocity data have been shown to be load- (preload) dependent to some degree (31, 36). Then strain rate measurements would be expected to be too. A recent study seems to confirm this with regard to strain rate propagation (37). At present, there is no specific data on the effect of afterload on strain rate measurements. As there were statistically significant differences in blood pressure, this may to some extent have influenced the results. Further studies both of patients with different load condition, as well as invasive animal experiments may be indicated.

5.2. Methods.

5.2.1. Validation

The relation between longitudinal velocity gradient and "true" strain rate is discussed in more detail in appendix A. In a clinical setting, this is of minor importance. Measurements are method dependent in any case. The main objective of this study has been to validate findings rather than actual measurements. Subsequent studies have validated integrated strain against microsonometry (38) and found a good correspondence. The validation in patients, however, still poses some problems. As discussed previously, the annulus velocity may be seen as the sum of all strain rates along the wall from the base to the apex. If peak strain rates are reasonably simultaneous, and colour SRI seems to indicate that they are, a peak systolic strain rate of 1.4 s^{-1} should, in a normal ventricle of about 9,5 cm give an annular systolic velocity of 13.3 cm/s. This exceeds reported normal values (10, 30) as well as the findings in paper 4. The explanation for this may be that the peak is less simultaneous than apparent from colour. In addition, the peak strain rate may be overestimated due to noise artefacts. When identifying the peak systolic strain rate, the chosen value will often include a high noise component, contributing to the peak value. True peak strain rate value may therefore be lower than the measured strain rate. When strain is concerned, however, this does not apply. The peak strain is the end resultant of wall shortening, i.e. the end systolic shortening, regardless of the timing of peak strain rate or velocity. This means that the peak strain should be end-systolic, and hence, simultaneous. In addition, when adding the instantaneous strain rate values as in equation 4, the effect of random noise will theoretically cancel out. As the noise is random there will on the average be as much noise subtracting from the true strain rate value, as there

will be noise adding to it. In a recent study (39), the normal value is reported as 16% shortening. In a normal ventricle this will amount to about 1.5 cm shortening of the ventricle, very close to the normal systolic annular displacement (4, 5, 6, 7, 8, 9).

In comparing strain rate imaging to 2D echocardiography, it is important to note that the 2D recordings were optimised, both in using second harmonic, as well as using an expert reader. This means that in paper 2 and 3 the reference method is as optimised as it can get. In contrast, using the tissue picture from the SRI cine loops is not optimal. The tissue picture underlying the colour SRI or DTI recordings has substantially reduced the number of lines in order to achieve higher frame rate. In analysing Doppler data, frame rate is the main priority, but the spatial resolution of the tissue picture has to be sacrificed. In a recent study (39) this resulted in a reduced accuracy of 2D echo compared to SRI and to the accuracy in paper 3, but the precision of SRI was similar to the one in paper 3.

The studies in paper 2 and 3 does show the main findings of reduced segmental function by echocardiography and SRI to give a moderate to good correspondence (28), in addition to performing similarly in relation to angiography. The moderate correspondence, however, seems to be mainly the result of the inherent precision of either method. The intra method variation is as great as the between method variation, as shown in table 4.

Table 4: Inter and intra method variability:

<i>Comparison</i>	k– coefficient	95% confidence interval	weighted k–coefficient
SRI vs. 2D - echo	0.52	0.41 - 0.64	0.64
2D-echo intraobserver	0.58	0.47 - 0.69	0.70
2D-echo interobserver	0.64	0.54 - 0.74	0.74
SRI intraobserver	0.66	0.56 - 0.76	0.75
SRI interobserver	0.47	0.35 – 0.58	0.60

The interobserver study of SRI is with the same two observers as in paper 2. In the first study after 5 learning cases, it was 0.32 (0.1 – 0.36), weighted 0.49, in this study with the previous 15 as learning cases, it was 0.47 (0.35 – 0.58), weighted 0.60. The improvement, may be taken as an indication of a learning curve for SRI.

Combining the results from paper 2 and 3 gives 30 patients. Of 451 segments, 336 had the same WMS by both methods, 92 differed by one degree, and 20 by two degrees:

Table 5: Segmental comparison between 2D echo and SRI:

		SRI					
		WMS	1	2	3	4	Sum
2D Echo	1		266	25	9		300
	2		24	39	11	3	77
	3		8	25	34	6	73
	4				1		1
	Sum		298	89	55	9	451

This gives a $\kappa = 0.50$ (0.38 – 0.61), weighted 0.63 (0.52 – 0.74).

5.2.2. Applicability

In general, Doppler shift is considered more robust than tissue echo, giving fewer dropouts. In the combined population in papers 2 and 3 however, a total of 30 patients with a possible yield of 480 segments, 473 were evaluable by 2D, 454 by SRI. In this preliminary work, no segments were evaluated that did not show either tissue lines or the propagation of strain rate during atrial systole. The intention of this, was to reduce the false interpretation of dropouts as akinesia. This rather restrictive practice was due to the method being new, with caution as well as lack of experience, as we were still learning the new method. On the other hand, some of the readings by 2D echo may be subconscious extrapolations of neighbouring segments, based on the considerable experience of the reader. What the studies seem to show, though, is that 2D echo performs well with state of the art imaging technique and with experience.

The analysis in this study was limited to the 16-segment model, and the 4-grade scale to be able to compare with 2D echo. Actually the temporal and spatial resolution of colour M-mode is better than 2D-echo, so the heterogeneity of systolic function within segments is better visualised. This may give hope of better sensitivity for minimal function, i.e. for viability.

This however, needs further research.

Peak systolic strain rate was measurable in 1012 of 1184 (85%) of the possible segments in papers 3 and 4.

5.2.3. M-mode measurements

In measuring strain rate propagation, a straight line M-mode was used, rather than the curved. In placing a curved M-mode, the curvature and hence, the length, is subjective. In accordance with this, the curved M-mode in the software application did not calculate distances, although it could be made to by some trickery. To avoid the subjectivity, the straight line M-mode was chosen. To compensate for the difference between the curved wall and the straight M-mode

line, the propagation velocity was measured in the basal half of the walls, where the wall was reasonably straight. However, the findings in paper 4, that the propagation velocity was apparently increased in the wall showing increased curvature in the base, indicates that a curved M-mode that follows the wall closely, would be the most correct, if there was a method to standardise, as discussed in 5.3.2. The measurement of apical delay of relaxation, as proposed recently (37), might solve this. Being a measure of the time interval only, it is curvature independent. However, this delay is level (base-midwall-apex) dependent, and the level of measurement need to be standardised instead. This method, however, poses additional problems. In the first case, the isovolumic relaxation of the apex may be misinterpreted as the relaxation during early filling. In the second case, if the delay is measured too near the apex, the angle dependency may be the limiting factor, as strain rate approaches zero as the angle increases (5.6.6).

The propagation velocity measurement has assumed the propagation velocity to be constant, as the measurement is linear. There are no actual data in the studies to support this, except for the visual impression.

Strain rate propagation has limited precision, the intraobserver limits of agreement in paper 4 were (-29.4; 32.5 cm/s) and interobserver limits of agreement are (-24.2; 36.6 cm/s).

5.2.4. Flow propagation measurement

The actual value of flow propagation velocity depends on whether front velocity (black-to-colour transition (32)), front of aliasing velocity (41, 42) or main direction of aliased flow (23) is chosen. In addition, measurements are dependent on scanner settings: Black-to-colour transition depends on the level of low velocity rejection, the aliasing contour on PRF.

Comparing different studies is therefore difficult, as shown by the variety of normal values given (23, 32, 33). Flow propagation was measured in the same files with an interval of one year, by the same investigator. The intraobserver limits of agreement was (-33.3; 52.1 cm/s), showing a rather low precision. The difference between patients and controls, and the negative correlation with strain rate propagation velocity, however, remained significant. To see if the method of measurement of flow propagation velocity would change the findings, both black-to colour and main direction of aliased velocity was measured as well. The comparison is shown in table 6. It is obvious from the table that the other methods of measurements have even less precision. In black to colour analysis, the differences between patients and controls, as well as the negative correlation between flow propagation velocity and strain rate propagation velocity are still significant. In main direction of aliased velocity measurements, neither difference nor correlation is significant, but the tendency is in the same direction. It is to be emphasised that flow analysis is limited to the linear measurements of the column flow. Neither delay of filling at the apex (43), nor eigenvector analysis (23) are done.

Table 6. Comparison of flow propagation by three methods.

	Front of aliased velocity	Black to colour transition	Main aliased velocity
Patients	54.8	55.5	72.1
SE:	1.59	5.11	11.72
Controls	69.9	144.1	137.2
SE:	3.75	30.60	32.18
P:	< 0.002	< 0.02	0.08 (NS)
R: (95% CI)	-0.57 (-0.79 – -0.23)	-0.43 (-0.7 – -0.04)	-0.19 (-0.54 – 0.22)

SE: Standard error of the mean. P: significance of the differences between the two groups.

5.3. Findings

5.3.1 The normal strain rate pattern:

From colour M-mode of the normals, a typical pattern is apparent:

Isovolumic contraction period is apparent as a simultaneous shortening. No propagation due to the electromechanical delay is apparent. Systolic shortening in the ejection phase starts virtually simultaneous in all levels, although the peak strain rate may be less simultaneous, as discussed in 5.2.1. In comparison with the tissue velocities, it is apparent that while the velocities decrease from the base to the apex (17) as shown in fig. 5 and 7a), that the peak strain rate is the same at all levels as seen in fig. 7b).

At end ejection there is an elongation wave starting at the midwall level. This has been taken as an indication of the isovolumic relaxation. In a recent study, however, we have shown that this wave occurs before closing of the aortic valve by phonocardiography (44). This corresponds to the established finding of protodiastolic filling (45) which again corresponds with the short period of reverse flow in the aorta before aortic valve closure as demonstrated by Doppler measurement (46). The finding that the elongation starts at the midwall level, however, must not be taken as an indication that relaxation starts here. MR has shown the initial diastolic deformation to be an “untwisting”, starting in the apex (15). This rotational movement will not show up in the longitudinal strain rate measurement, unless resulting in a visible elongation of the ventricle. This will be more apparent in the midwall part, where the shape of the ventricle is more cylindrical. The finding may therefore only represent the first visible diastolic deformation by longitudinal strain rate.

In diastole, unlike the early and late diastolic peak tissue velocities, the peak strain rates of the two phases do not decrease from the base to the apex. On the other hand, while peak early and late velocities are simultaneous at the different levels, the peak strain rates are delayed from the base to the apex as shown in fig. 7b). This is also shown in the colour M-mode as a wave

of elongation. The propagation velocity of these waves is the same in all walls, in the normals. As the mitral valve opens, the part of the walls closest to the valve are the first to move. The propagation of the wall elongation may then be similar to a queue of cars starting to drive. While the cars moves forward, the starting of the cars is a wave propagating backwards. In the colour M-mode in paper 4 and in the curve sequences in fig 7b) is seen that the elongation waves return from the apex, this can also be discerned as a small oscillation of the mitral ring when studied by pulsed tissue Doppler. The returning wave is of low amplitude, and may be difficult to discern from the noise in the strain rate curves. The returning wave may be either a reflection, or, as the apex is dome shaped and retreating from the chest wall during this phase, more probably the continuation of the wave from the opposite wall. The diastasis is a period of no deformation, and finally atrial systole is a new wave of elongation propagating from the base to the apex and returning to the base. As the atrium in the late diastole actually pulls on the mitral ring, the propagation from the base to the apex can be easily explained.

5.3.2 Systolic function

The comparison between 2D echo and Colour SRI does confirm that SRI shows regional deformation of the myocardium.

The studies in normal subjects, and the symmetric ventricles of the hypertensive patients do all show the same peak systolic strain rate in all levels of the ventricle i.e. basal, midwall and apical. This means that the longitudinal systolic velocity gradient is constant along the ventricle, if the peak strain rate is simultaneous, which is not proven, but may seem reasonable from experience.

Another implication of the results in paper 3, is that wall thickening and wall shortening seems to convey the same information, i.e. to be interchangeable. This means that they are inversely related, as is hypothesised in fig. 2 and 4. In other words, as the wall shortens it thickens, as it stretches, it thins, confirming the conservation of volume, to a certain extent. There are no established normal values in for longitudinal strain rate so far. The normal values in this study, compared to the hypertrophic and infarcted patients are given in table 7.

Table 7. Mean peak systolic strain rate of normal subjects, hypertensive patients and myocardial infarction grouped according to Wall motion score by 2D echo.

Subjects: (Number of patients/Number of segments)	Peak systolic strain rate (s^{-1}) (Standard deviations)
Normal controls (N = 28)	1.43 (0.21)
Hypertensive patients (N = 26)	1.15 (0.17)
Myocardial infarctions (N = 20)	1.00 (0.56)
WMS = 1 (N = 200)	1.21 (0.42)
WMS = 2 (N = 44)	0.77 (0.51)
WMS = 3 (N = 49)	0.38 (0.53)
WMS = 4 (N = 1)	0.00 (NA)

5.3.2. Diastolic function

Peak diastolic strain rate may be an assessment of the rate of relaxation. The finding of the propagation waves of the wall elongation during the filling phases, however, adds information about the physiology of diastole. When the fact that wall thinning and stretching are inversely related is coupled to the finding of the propagation of the elongation, this may also be seen as a wave of chamber dilation as illustrated in fig. 9. The propagation velocity of the chamber dilation is the strain rate propagation velocity of early diastole (PVSe). This is the rate of chamber expansion as well, and thus, related to the rate of filling. In delayed relaxation, both peak strain rate and the propagation velocity of strain rate in early relaxation is reduced. The tissue velocity of the mitral annulus is reduced as a consequence of both. Reduced peak strain rate will result in a direct reduction of peak velocity. Reduced propagation of peak strain rate will result in increased temporal dispersion of peak strain rates, resulting in a lower and wider velocity curve, with reduced peak. Propagation velocity of strain rate is the same in all six walls of the standard apical planes in the normals. An implication of the documented non-simultaneity is that the diastolic strain is non-uniform at any specific time along the wall, even if the peak values are equal.

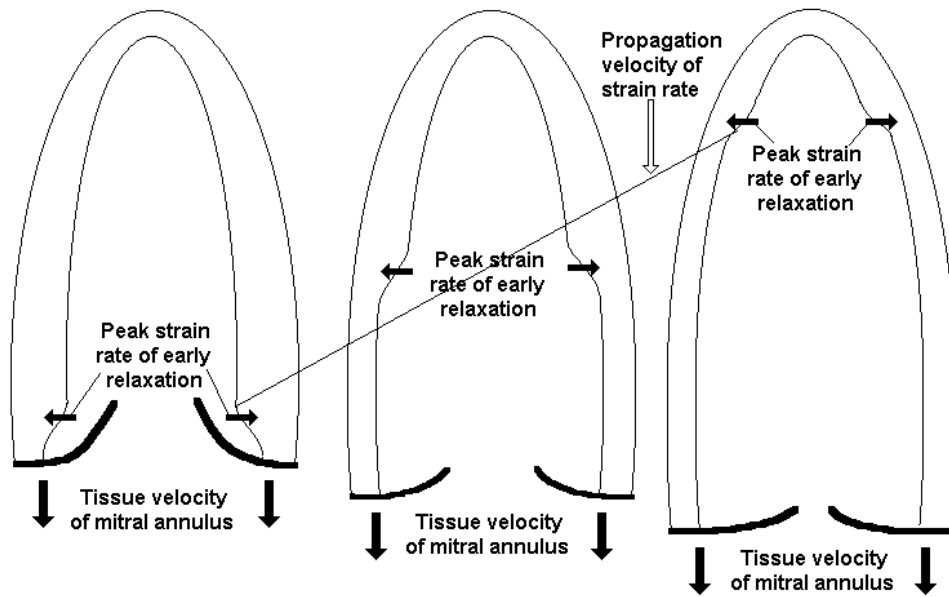


Fig. 9. The wall stretching in early filling propagates from the base to the apex. A wall stretching implies wall thinning, this means that the chamber expansion due to wall thinning propagates from the base to the apex as well. The propagation velocity in this diagram is the slope of the thin line crossing the three phases of early filling. It corresponds to the propagation velocity of strain rate.

Table 8. Peak systolic and diastolic strain rate at different levels in normals:

Level:	PSR_S (s^{-1})	PSR_E (s^{-1})	PSR_A (s^{-1})
Apical	1.44	2.43	1.37
Midwall	1.42	2.13	1.29
Basal	1.42	2.39	1.47
Global	1.43	2.30	1.38

PSR_S : Peak strain rate in systole, PSR_E : Peak strain rate of early filling, PSR_A : Peak strain rate of early relaxation.

Table 9: Peak systolic and diastolic strain rate, and diastolic strain rate propagation velocity in different walls of normals:

<i>Wall</i>	PSR_S (s ⁻¹)	PSR_E (s ⁻¹)	PSR_A (s ⁻¹)	PVS_E (cm/s)	PVS_A (cm/s)
Septal	1.46	2.29	1.69	60.6	90.6
Anteroseptal	1.37	2.10	1.56	56.8	88.2
Anterior	1.42	2.29	1.47	59.3	92.7
Lateral	1.38	2.30	1.44	63.1	98.7
Inferolateral	1.50	2.32	1.38	60.0	93.6
Inferior	1.37	2.27	1.38	59.2	102.1

PVS_E: Strain rate propagation velocity of early filling. **PVS_A**: Strain rate propagation velocity of atrial systole.

Differences between the walls were not significant by ANOVA analysis, showing normal systolic and diastolic function to be symmetric.

The finding of increased propagation velocity in the anterior septum of the patient group is probably due to an artefact, as the hypertrophic wall is s-shaped, increasing the difference between the wall length and the straight line M-mode line. This gives an apparently reduced wall length, and thus an apparently increased velocity. Global peak mitral annulus velocities, peak strain rates and propagation velocities of strain rate in early and late diastole are given in table 10, for both controls and patients.

As both tissue Doppler measurements (31, 36) and strain rate propagation velocities (37) have been shown to be preload dependent, invasive studies to establish the relation between the separate components and load is indicated.

Table 10. Peak annulus velocity, peak Strain Rate and peak strain rate propagation velocity of early and late filling. (Standard deviations.)

	<i>DTIe</i>	DTIa	PSRe	PSRa	PVSe	PVSa
	(<i>cm/s</i>)	(cm/s)	(s⁻¹)	(s⁻¹)	(cm/s)	(cm/s)
Controls	13.1 (2.8)	10.2 (1.8)	2.22 (0.49)	1.49 (0.48)	60.0 (12.9)	94.0 (22.1)
Patients	8.2 (1.5)	11.0 (1.8)	1.46 (0.25)	1.66 (0.37)	31.6 (9.3)	72.0 (16.2)
P:	<0.001	NS	<0.001	NS	<0.001	<0.001

DTI: peak annulus velocity by pulsed Doppler of E – and A – wave. PSR: peak strain rate of E – and A – wave. PVS: propagation velocity of strain rate of E – and A – wave.

5.3.3 Flow measurements

As discussed in the previous paragraph, the strain rate propagation velocity may be a measure of the rate of chamber expansion, and hence, filling. As strain rate propagation is reduced or delayed, an increase in the filling time is to be expected. The finding of an inverse relation between strain rate propagation and deceleration time of mitral flow as shown in fig. 10 supports this, as deceleration time of early mitral flow is a measure of the filling time of early diastole. Strain rate propagation shows similar values in normals as previously reported for flow propagation (23). In paper 5, the strain rate propagation and flow propagation velocity are similar in the normal subjects as well.

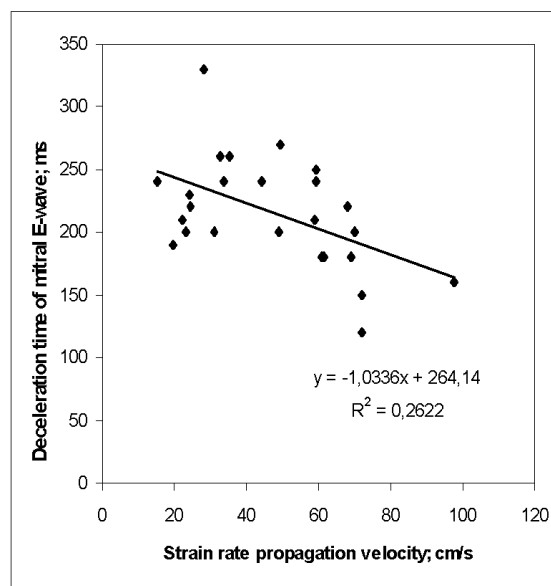


Fig. 10. Scatterdiagram of the relation between strain rate propagation velocity and deceleration time of mitral flow. As the chamber dilation propagates slower, it means that the rate of chamber expansion decreases and the filling time increases. An inverse relation between the two is expected.

On the basis of this, a model of normal filling as in fig. 11 can be proposed. In-flowing blood is deflected from the front of the flow wave to fill the void created by the chamber expansion. The flow front propagates backwards in the inflowing blood column and thus the propagation velocity is less than the flow velocity. In delayed relaxation, it could be expected from this model that both strain rate propagation and flow propagation velocity would be reduced. This would also be in accordance with previous studies (23, 32, 33, 41, 42, 43).

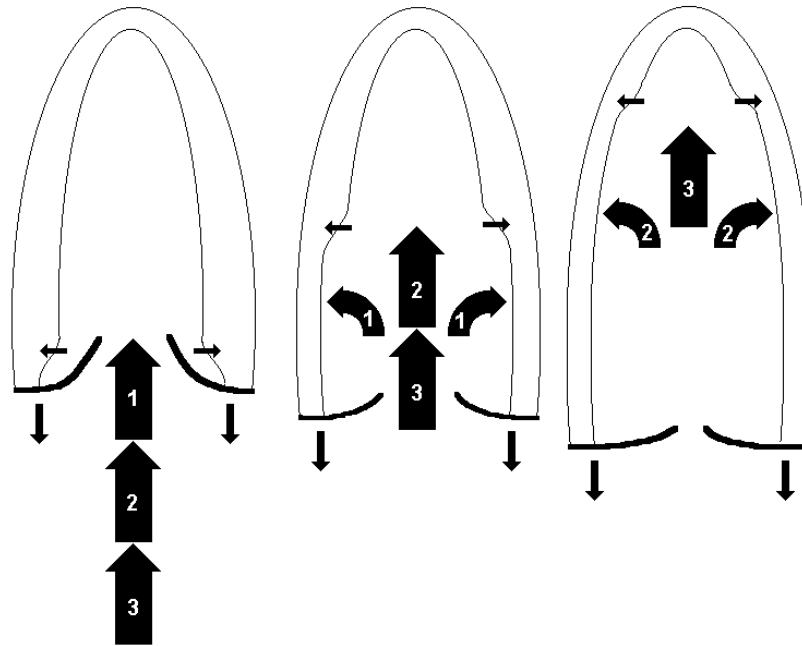


Fig. 11. Proposed sequence of events during normal filling. As the ventricle widens, the foremost part of the flow column is deflected to fill the expanding chamber. This means that the velocity front propagates backward relative to the in-flowing blood column, and with a lower velocity than the flow velocity. The flow propagation is illustrated by the propagation of the foremost arrow (1 – 2 – 3), while the flow velocity is represented by the propagation of arrow n° 3. The diastolic motion of the base of the heart deflects the blood further, resulting in vortex formation (not shown in figure).

The finding of the opposite relationship was surprising. The most robust finding is that the flow propagation velocity was increased in a population with delayed relaxation. In accordance with this, there was a negative correlation between flow propagation and strain rate propagation velocity in the whole study group as seen in fig. 12. From the scattergram, it is also obvious that this is not due to clustering of the results, as measurements are spread out over the whole range. We had to consider the differences between the study population and those of previous studies.

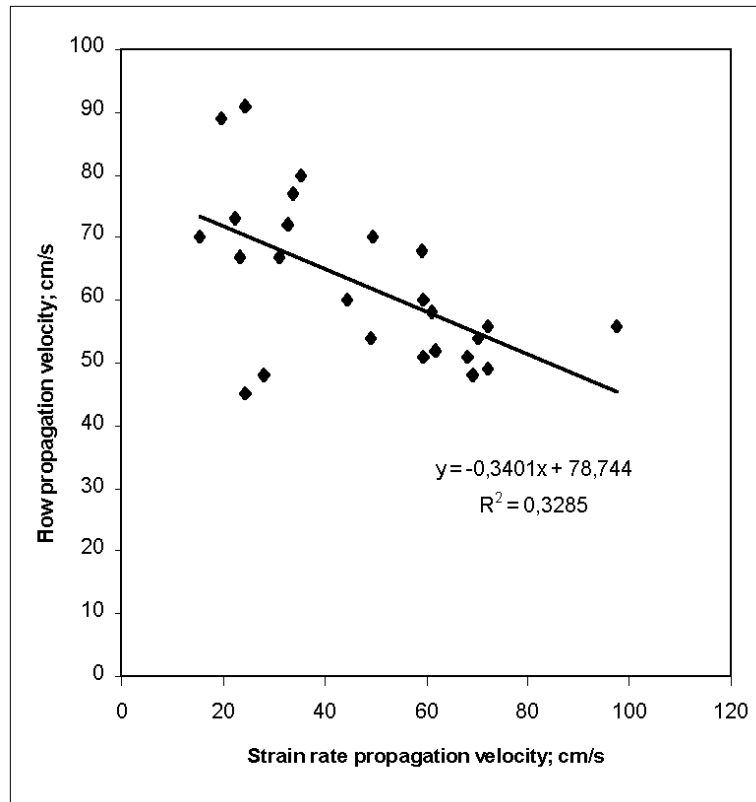


Fig. 12. Scatterdiagram of the relation between strain rate propagation velocity and flow propagation velocity, showing the inverse relation.

In a previous model experiment, Steen & Steen (47) does show that flow propagation velocity is partly a function of the annulus / chamber diameter ratio. These model experiments, however, did not take into account the dynamic nature of left ventricular deformation during early diastole. In our study, there was no significant difference in end diastolic diameter between patients and controls. But when early filling phase is seen as a dynamic event, there are transient differences in diameter as shown by the delayed strain propagation. Slowing of strain rate propagation means that the ventricle remains narrow for a longer time during early filling. Many of the previous studies do not report the systolic function or the ventricular diameter. Animal studies may be confounded by the change in left ventricular geometry induced by the open chest procedure.

In a recent study of flow propagation in hypertrophic cardiomyopathy, however, flow propagation is reduced (48). No ventricular diameters are reported, but the ventricles are described as hyperdynamic. A recent MR study of flow in normal subjects reports decreasing velocity propagation with increasing age (49). In none of these populations is there any reason to assume any chamber dilation. The findings in the present study are not in accordance with the findings in those studies.

The patient group has delayed relaxation, as evidenced by the prolonged deceleration time and IVR (22) as well as reduced early diastolic mitral annulus velocity by tissue Doppler (31). On this background, peak mitral flow velocity and E/A ratio of mitral flow is higher than expected in a group with delayed relaxation. There is no significant reduction in peak mitral flow velocity, and although there is a significant reduction in E/A ratio of mitral flow velocity, it is about 1.0. The flow and strain rate findings are summarised in table 11. There is no reason to assume that this finding of a high mitral flow velocity is due to increase in filling pressure with pseudonormalisation. Firstly, there is no evidence of pseudonormalisation in the patient characteristics. As the deceleration time and IVR is prolonged and the average MVmax/DTE (E/Ea) ratio in the patient group is 8.0 (50), there is no reason to assume increased filling pressure and pseudonormalisation, but rather very moderate pathology. Secondly, flow propagation has previously been reported to be load-independent (48, 51), so preload alterations should not explain the flow propagation increase in any case.

Table 11: Mean strain rate and flow measurements. (95% Confidence intervals)

	PSR_E (s ⁻¹)	PVS_E (cm/s)	PVF_E (cm/s)	MV_{max} (cm/s)
Controls	2.21 (1.91 – 2.50)	66.6 (59.9 – 73.4)	54.8 (51.6 – 57.9)	73,6 (63.6 – 83.9)
<i>Patients</i>	1.51 (1.38 – 1.63)	29.6 (24.3 – 34.8)	69.9 (62.6 – 77.3)	64.9 (56.1 – 73.7)
P:	<0.001	<0.001	<0.002	NS

PSR_E: Peak Strain Rate during early filling, **PVS_E**: propagation velocity of strain rate during early filling, **PVF_E**: propagation velocity of flow during early filling and **MV_{max}**: peak early transmitral flow velocity.

In table 11, it is evident that there is a high mitral flow velocity and a very similar flow propagation velocity in the patient group. Coupled to the finding of a reduced strain rate propagation velocity, a model of filling as shown in fig 13 could be proposed. As the inflow velocity is higher than the propagation of camber dilation, the inflow will be forced forward, as shown. The flow propagation may then be equal to, or even exceed (by convergence) the flow velocity at the inflow. At the same time, the relaxation is shown to have begun at the apex, giving a gradient for direct flow into apex (15).

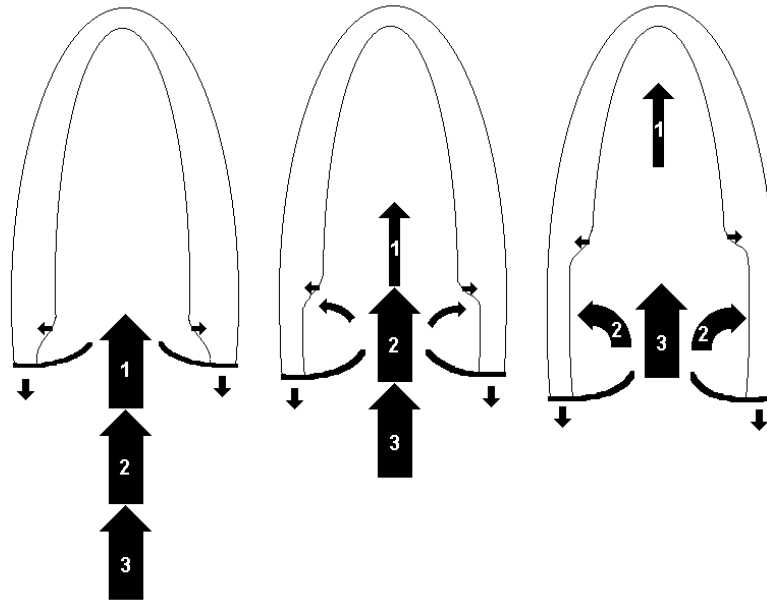


Fig. 13. Proposed sequence of events during early filling in patients to account for the findings. In delayed relaxation, strain rate is shown to propagate at a lower velocity, resulting in less deflection of blood from the column front, and hence, a flow propagation velocity that approaches the inflow velocity.

Assuming a decrease in peak inflow velocity, the proposed sequence of events in fig 12 might reverse. With a reduced inflow velocity, the chamber expansion would keep up with the flow velocity (filling rate), and the sequence of events in fig 11 may again dominate at a slower rate. In this case, flow propagation and strain rate propagation will synchronise again.

By this model, flow propagation should be a function of both inflow velocity and strain rate propagation. This is supported both by the multivariate analysis showing the interaction between mitral flow velocity and strain rate propagation as determinants for flow propagation (table 12), as well as the correlation between MVmax/PVSe and flow propagation velocity (fig 14). When diastolic diameter, however, it should be considered that there is a narrow range of variation, within normal limits.

Further research will be needed to examine this interrelationship over a wide range of values. Flow propagation alone may have too many determinants to be a simple index of diastolic function. Neither strain rate propagation nor flow propagation velocities do at present show the precision necessary for clinical use.

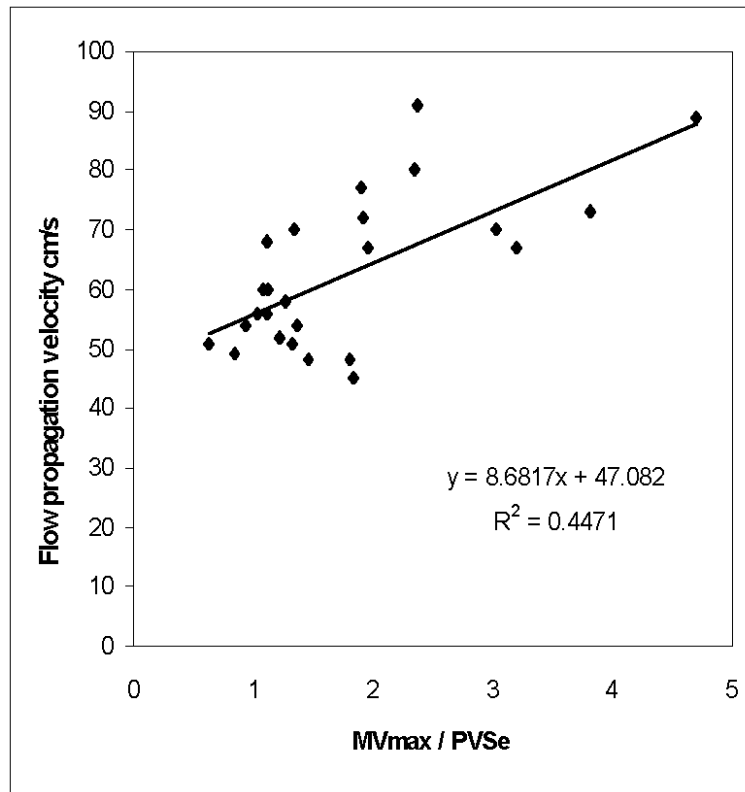


Fig. 14. Diagram of the relation between flow propagation and the ratio between mitral flow velocity and strain rate propagation. The low R^2 indicates that the relationship is not linear, however.

Table 12. P values for relation by linear regression. PVFe as dependent variable.

	All	LVDd	DTIe	Dec-t	IVR	PSRe	PVSe	MVE
Univariate	—	NS	NS	NS	NS	NS	0.003	NS
Multivariate (all)	0.016	NS	NS	NS	NS	NS	0.004	0.017
Multivariate PVSe, MVE	0.001	—	—	—	—	—	<0.001	0.014

5.4. Limitations of the studies

The study has not validated strain rate imaging as true strain / strain rate, as would be the case in model experiments or direct comparison with MR, but as assessment of regional wall function in a clinical setting. The limitations this gives in the validity of measured values may be more theoretical than of clinical relevance, however. On the other hand, if the measurements in this study incorporates a high noise component, the results may not be representative for measurements if SRI is improved concerning noise.

As discussed in 5.2.1, in paper 2 and 3, two imprecise methods are compared as validation. The correspondence between methods and thus, the actual validation is limited. Only semi-quantitative strain rate is in fact validated, but this is due to the chosen reference method being semi-quantitative as well. In paper 2, no attempt is done to quantify the measurements, and in paper 3, only peak systolic strain rate and not strain is measured. This means that the actual precision of peak strain, as well as the applicability (by the number of measurable segments) can not be estimated.

The precise relation of longitudinal vs. transverse strain is subject to mathematical analysis and dependent on the presence of shear strain as well as the magnitude of circumferential strain. The relation that has been established in this study is only semi-quantitative.

The actual method of measurement of strain rate propagation velocity is open to question. The propagation velocity may not be constant, and thus the equation not linear as assumed, as discussed in section 5.2.4.

The low numbers limit the study of flow propagation velocity. Even though there is significance, other determining factors for flow propagation may be found as not significant because of small variations in the limited population.

5.5. Advantages of the strain rate imaging method

Strain rate imaging is the first method for true quantitation of regional function by ultrasound. Velocity measurements are influenced both by translation of the whole heart and the tethering effect of the neighbouring segments. The tethering is in fact the mechanism for the gradual increase in velocities from apex to base. But tethering means that even akinetic segments may have velocities, as shown in papers 2 and 3. Annular velocities may even be normal, as contracting segments may be hyperkinetic. By utilising velocity differences, both tethering and translational velocities are simply subtracted.

Even though echocardiography and SRI seem to yield the same information in the studies in papers 2 and 3, there are some advantages of colour SRI:

Even though the two methods do seem to give equivalent information, colour assessment is a completely different way of visualising the data. With SRI, both colour and motion

information is accessible; at least if double loops are recorded as in papers 2 and 3. This means that the information in cases of uncertainty, the interpretation may be easier, especially to less experienced. The learning curve of colour strain discussed in 5.2.1. may be an indication of this.

In grey-scale assessment, correct interpretation is dependent on correct mid-chamber plane or else the wall motion and thickening may be exaggerated as shown in fig. 15. The deviation in strain rate measured from the apex is less, if the plane deviates from mid-chamber, as the deviation is perpendicular to the tissue velocities.

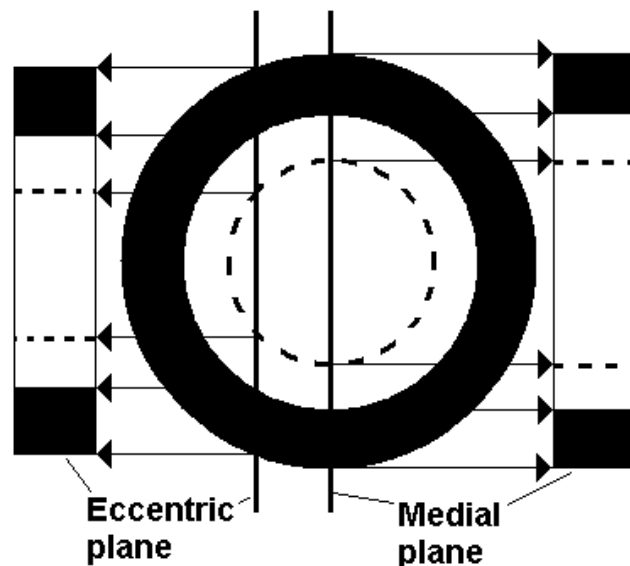


Fig. 15. Illustration of the geometric distortion of 2D echo. The filled circle is the myocardium in diastole. The broken line is the endocardium in systole. To the right is the projection of a correct mid-chamber plane, giving the correct wall thickness, thickening and chamber diameter. To the left is the projection of an eccentric plane, showing how this leads to an overestimation of wall thickness, wall thickening and chamber shortening.

A study of interpretation of computer generated delayed onset of segmental contraction in 2D echo cine-loops, has shown that the detection of delayed onset contraction is reliable only if it is more than 100 ms, and is definitely unreliable below 80 ms. (52). In SRI this delay can be measured directly in the M-mode with time resolution up to the maximum frame rate. Post-systolic shortening is shown to be a very early marker in acute myocardial ischemia (53). The demonstration of post-systolic shortening may increase the sensitivity as well as the precision of stress echo, beyond mere measurement of regional systolic contractility. Both

presence and location of post-systolic shortening is easy to demonstrate with SRI. Its universality in myocardial infarction however, leaves open to discussion whether it really is a viability marker (54).

The main advantage of strain rate imaging is its potential availability. With capacity for colour DTI, the algorithm is so simple that it can be implemented in real-time processing without the need for any additional processing capacity. Thus, it can be available bedside, in contrast to MR and complicated post-processing.

Strain rate imaging has today a high temporal resolution, with a frame rate of up to 130 FPS, i.e. a temporal resolution of 8 ms. This may be close to what is needed to study the short duration of the isovolumic phases, as well as arrhythmias and conduction disturbances.

5.6. Limitations of the strain rate imaging method

5.6.1. Aliasing

If one of the velocities used to calculate strain rate is aliasing, the resultant strain rate is also false. Theoretically, if v_1 is aliased, the resulting velocity difference should increase. If v_2 is aliased, the resulting velocity difference should decrease or reverse. If both velocities alias, however, the velocity difference remains unchanged, and no aliasing of strain rate occurs. In practice, aliasing in most instances results from noise added to velocity measurements, so it is still open to question whether there is less aliasing in SRI than in DTI. Typical aliasing in strain rate and strain curves is shown in fig. 16 c) and d), and in colour strain in paper 3, fig. 9. If the M-mode line is not within the wall, velocities and turbulence of blood may give high strain rates with aliasing as well.

5.6.2. Reverberations

Reverberations may also give rise to false inverted colours, as strain rate is calculated in relation to apparent immobile echoes. It will ordinarily show up in the M-mode as a horizontal line of inverted colour.

5.6.3. Noise

The strain rate method has serious noise problems. This is illustrated in Fig. 16. The numerical derivation of the gradient is noise sensitive. As strain rate is based on the difference between two velocities, while the error is the sum of the errors of the two velocity measurements. The noise to signal ratio is thus far more unfavourable than for velocity measurements alone. In quantitative strain rate imaging the noise may give too high peak values as previously discussed (5.2.1). The low accuracy seen in paper 3 is due to this. In addition to temporal smoothing of the curve, smoothing can be achieved by different means.

A method of decreasing noise is to increase offset length. As the noise is considered random, increasing offset length will increase the velocity difference and the distance in equation 7). The velocity difference will increase, and the noise-to signal will decrease, in proportion to the increase in Δx . The velocity gradient will remain unchanged as both the velocity difference and the offset length increase in the same proportion. Increasing the offset length will in fact give a (temporal) smoothing of the strain rate, but on the cost of reduced spatial resolution (fig. 16c). If the 16 segment model is used, however, where only the segmental function need to be considered, a radial resolution of 1.5 cm (to avoid the angle problems at the base and the apex) may be sufficient. The studying of transmural strain, however, will be limited by the noise. Ideally, the offset should be equal to the minimum wall thickness, (5-7 mm). As the wall moves, however, it will have to be even less, to keep the whole offset length within the wall during the whole heart cycle. It may be feasible in the posterior wall, but the motion of the septum may demand an offset length that may be prohibitive because of noise. The high noise components may account for some reports showing very high strain rate values, even in akinetic segments (55).

Another way of temporal smoothing is to integrate the strain rate to cumulated strain (fig. 16 d). As noise is random the integration will tend to eliminate the noise by evening out as discussed in 5.2.1. Integrated strain may thus be a method of using shorter offset lengths.

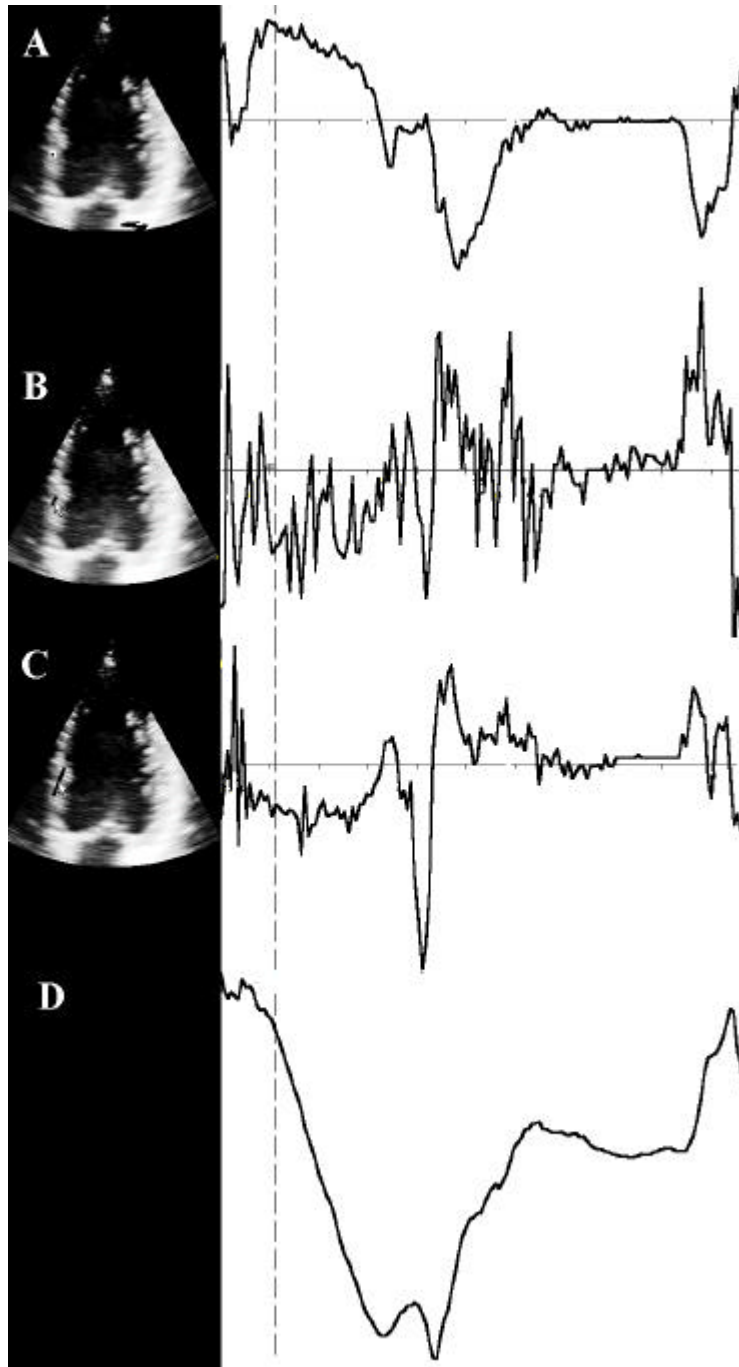


Fig 16. Noise sensitivity of strain rate measurements. All measurements are from the same clip.

- A.** Velocity curve from the point indicated on the 2D image.
- B.** Strain rate curve from the same area. The offset distance (Δx) is 5 mm. Both the area and the offset length is indicated on the 2D picture.
- C.** The effect of increasing the offset length to 15 mm. The length is show on the 2D picture, indicating the loss of spatial resolution. The curve is much less noisy, although a spike is seen at end ejection which is aliasing due to noise.
- D.** Integrating the strain rate curve of C to strain will smooth the curve further. The aliasing artefact is still visible, though. The temporal smoothing gives loss of time resolution.

5.6.4. Frame rate:

The frame rate of SRI in most of the studies has been around 70. In the early experimental stages, it was uncertain whether the tissue information was important for the interpretation. Colour DTI can achieve a framerate of 130 when the whole ventricle is kept in the sector, and off-line SRI from DTI has the same. The same framerate can be applied in online SRI, but on the cost of tissue resolution. Personal experience indicates that the high framerate will reduce noise, probably due to the increased number of points on the strain rate curve, indicating that the maximal obtainable frame rate is the optimal. If tissue resolution is an issue, the answer will then be to acquire two sets of data, 2D second harmonic as well as tissue Doppler or strain rate. In the future, both velocity / strain rate data and tissue information may be calculated from RF data, with no trade off between the methods. It should then be possible to contain all information in the same loop.

5.6.5. Spatial resolution

The minimum distance, over which the strain rate can be measured, the offset distance (Δx in fig. 6) is limited by the accuracy of velocity measurements. The random error in the strain rate estimate is inversely proportional to the offset distance. Thus, the offset distance is a compromise between accuracy and spatial resolution. In the studies, offset distance of 5 to 7 mm, has been used. There may be different optima for different purposes, as discussed above. In any case, the spatial resolution is less than in DTI, as long as strain rate is measured over finite distances.

The lateral resolution is equal to the beam width, plus the amount of averaging. The lateral averaging was maximised, also to decrease noise, but reducing the possibility of measuring differences across the wall and thus changes in shear strain.

5.6.6. Insonation angle:

The strain rate is measured along the ultrasound beam, not along the direction of longitudinal strain. In velocity measurement, the measured velocity is reduced in proportion to the cosine of the angle between the velocity vector and the ultrasound beam α , with zero velocity at an angle of 90° . In strain rate imaging, this problem is accentuated. The velocity gradient is reduced by the cosine of the angle between the velocity vector and the ultrasound beam as velocity measurements. In addition, in an incompressible heart muscle, there is transverse strain in the opposite direction due to the conservation of volume, further detracting from the numerical value of strain rate. This is proportional to the cosine of the transverse angle, β , (the angle between the ultrasound beam and the transverse strain). It can be shown (appendix) that the measured strain rate (SR_m) is

$$9) \quad SR_m = SR (\cos^2 \alpha - \sin^2 \alpha).$$

where α is the angle between the ultrasound beam and the wall (the principal strain direction) when analysed in two dimensions. Strain rate is thus reduced to zero at an insonation angle of 45° as illustrated in fig 17. In three dimensions this will be already at an angle of 30° if the strain is equally distributed along the three directions (56). This, however, is dependent on the relation between the longitudinal and transverse strain to the circumferential. If circumferential strain is close to zero, as discussed in 1.2, the insonation angle with zero strain really will be 45° .

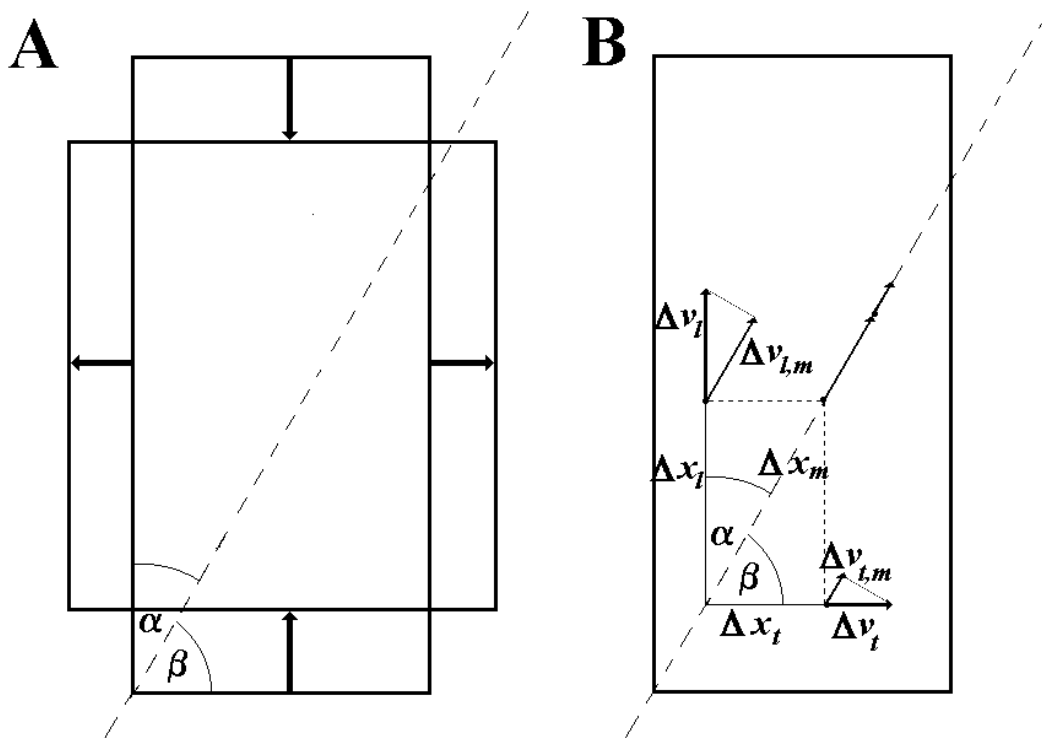


Fig. 17. Angle dependency of strain rate measurement. The dotted line illustrates the ultrasound beam, α is the angle between the ultrasound beam and the longitudinal axis, β is the angle between the ultrasound beam and the transverse axis. A illustrates an incompressible object, where the strain rates are simultaneous and with opposite values. The arrows indicate the longitudinal and transverse strain. It is evident that the longitudinal strain is reduced by the angle in the same way as the longitudinal velocity. In addition the transverse strain, being opposite, will detract further from the measured strain, so the angle detracts more from strain rate measurement than from velocity measurement. B illustrates that the measured velocity difference Δv is the sum of the longitudinal and transverse velocity component along the ultrasound beam, and the distance Δx is the projection of the offset distance along the ultrasound beam. It is shown in the appendix that the measured strain rate SR_m is related to the longitudinal (SR_l) and transverse (SR_t) strain rate: $SR_m = SR_l * \cos^2 \alpha + SR_t * \cos^2 \alpha$. Due to the incompressibility shown in a, the transverse strain is opposite, so $SR_l + SR_t = 0$. Then the strain rate is: $SR_m = SR_l (\cos^2 \alpha - \sin^2 \alpha)$. At an angle of 45° , the measured strain rate is zero.

The angle dependency may constitute a problem in the apical and basal segments. However, in our experience the basal parts of the apical segments and the apical half of the basal segments are parallel enough to measure strain rate with sufficient precision, as shown by the

unchanged peak strain rate at all levels. Another problem may be in septal hypertrophy in advanced age and hypertension, where the septum assumes a s-shape and the ultrasound beam may be almost transverse to the septum resulting in apparent a- or dyskinesia. This is mainly visible in the long axis view, not in the four-chamber view, and constitutes a serious pitfall in interpretation. The areas of greatest angle to the ultrasound beam are shown in fig 18. The right ventricle being more curved than the left in the long axis view may be even more prone to angular distortion.

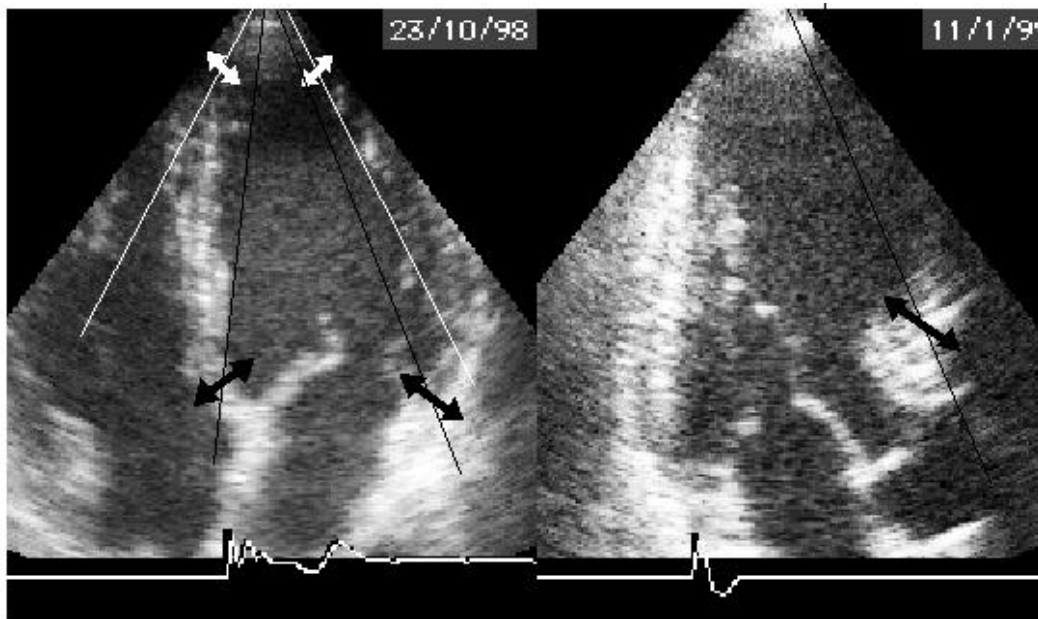


Fig. 18. Areas of the heart where the wall deviates most from the ultrasound beam, the apex, the base and the septum where it is S-shaped due to hypertrophy. The thin lines illustrate ultrasound beams, while the thick arrows indicate the transverse direction, where systolic thickening will be more parallel to the ultrasound beams, and thus give apparently inverted strain values.

5.6.7. One-dimensional measurement

Strain Rate Imaging allows measurements in one dimension at a time only, while strain has at least three, possibly up to nine components. As discussed in 1.2, in an incompressible body, strain in one direction has to be balanced by inverse strain in transverse directions. Thus the assumption of incompressibility (conservation of volume) makes it possible to extrapolate from one component to two. The findings in paper 3 supports this. If two strain components could be measured simultaneously, the third could likewise be inferred. On the other hand, the shear strain components are so far not accessible. The “twisting – untwisting” demonstrated by MR (15) is an example of this.

5.6.8. Strain is wall deformation

Finally, it has to be kept clear, that strain is a measure of deformation, not muscle function. The muscle contraction (sarcomere shortening) results in both shortening of the muscle fibres and wall segments and tension in the fibres / wall segments. In order to fully characterise muscle functions, the stress / strain relations would have to be measured analogous to the pressure / volume curves of global function. The local stress, however is not only dependent on local pressure and radius. The longitudinal load of a muscle segment is also a result of the contraction of the neighbouring segment. In regional dyssynergy, this mechanism alone may be responsible for reducing or delaying contraction, and even to the stretching of non-contracting segments, i.e. dyssynergy. This interrelation between the deformation of neighbouring segments is most easily visualised by colour SRI and this may introduce a new dimension in load considerations, regional pressure/strain loops may be a rather crude approximation.

Thus when deformations are described as contraction and relaxation, this is imprecise, as no load is considered. This means that strain measurements can not differentiate between contraction and recoil, between passive stretching and relaxation without additional information. When the action of neighbouring segments as well as the phase in the heart cycle is taken into account, this may be interpreted to some extent.

5.7. Strain rate or Strain?

It is important to realise that strain rate and strain measures different things. The rate of contraction may be slowed, but prolonging the contraction may compensate this, so the strain rate may be reduced while the total strain is not. Typically this is seen in the post-systolic shortening of acute ischemia (53), where the systolic strain during the ejection phase is reduced, followed by shortening after the closure (resulting in no useful work, though) after aortic valve closure. In increased heart rate, the strain rate may increase in response, but with shortening of systole the total strain may not, resulting in no increase in stroke volume. For assessing the total information, both strain rate and strain should be evaluated.

As discussed in 5.2.1 and 5.6.3, integrating the strain rate to strain will result in a smoothing of the time-curve and reduction in noise. As a result, the peak, or end-systolic strain should be both more robust and more precise measure of regional systolic function. The better correspondence between strain and annulus motion (39) than between strain rate and annulus velocity (5.2.1) may seem to confirm that. On the other hand, no direct comparison of reproducibility has been shown so far. In addition, the strain curves are prone to drifting of the baseline, due to various causes such as poor frame rate with missing of peak values, inhomogeneous strain within the sample volume, angle changes in the cardiac cycle or bias (3). The data has to be reassessed, with a direct comparison of the repeatability of strain rate

and strain, as well as the diagnostic accuracy before strain measurement can be proved more precise than strain rate.

Another drawback of integrated strain is the loss of temporal resolution. It may lead to the loss of sensitivity for post-systolic shortening as a marker of ischemia, and hence to loss in sensitivity in general. Only further examination of the data as well as prospective studies in stress echo will clarify that. For the timing of events in the heart cycle, strain rate is most appropriate, with time resolution equal to the frame rate. For timing purposes, quantitative strain rate measurements are not as necessary, so the noise is of less consequence, and colour strain rate will be the most appropriate, giving quantitative measurements of timing and depth.

5.8. SRI vs. DTI

The relation between colour SRI and colour DTI has been discussed previously (5.5). In addition, as already discussed, SRI is more sensitive to noise (5.6.3) and to angular distortion (5.6.6). In regional wall function assessment, i.e. in coronary disease, SRI gives more direct information of regional function than the corresponding velocity measurement, at least when the noise is acceptable.

For global function, however, the pulsed DTI is quick, easy and reliable. It is conceivable that the peak systolic velocity of the mitral ring, sampled from four points, will give comparable information about global systolic function (10) as the average strain rate sampled from 16 segments. When diastolic function is considered, the same applies to ventricles with symmetric function. The annulus diastolic velocities (14, 30, 31) incorporates the information about both peak strain rate and strain rate propagation in one measurement, and is quicker and much less cumbersome in daily clinical practice. On the other hand, the strain rate gives much more information about the spatio-temporal sequences in the ventricle, as discussed in 5.3.2. This information is at present mainly physiological, and the clinical value remains to be seen. Comparison of tissue velocities and strain rate curves is shown in fig. 8a) and b).

When regional function is considered, Tissue Doppler at one point of the mitral ring has been supposed to measure the function of one sector, and give regional information of dyssynergy of one wall. In a recent study (57), this is not confirmed. The variation between points on the mitral ring is not greater in infarction patients than in normal subjects. The reason for this is that the different vascular beds do overlap in different walls. This is shown by the loss of regional differences when the strain rates of all levels in each wall are summed. This leaves strain rate imaging to be the only true regional method.

5.9. Potential of SRI and future developments

Further research will determine whether strain rate imaging in its present form will suffice to give true quantitative stress echo. Greater precision may be achieved by various smoothing adjustments as well as optimising frame rate.

The temporal resolution of SRI is of interest in studying arrhythmias and conduction disturbances. Non-invasive location of start of both extrasystoles and pre-excitation may be feasible, and could prove useful in relation to ablation therapy.

The temporal resolution of SRI will give new, physiological information about the isovolumic phases. The clinical utility of this remains to be determined.

During most of diastole, the ventricular myocardium is passive. This means that mechanical events are a function of the load changes and the material properties of relaxed myocardium. The atrial systole is perhaps the most important, but experience has already shown that the deformation wave of the early filling phase continues or is reflected back toward the base during the first part of diastasis (paper 4). SRI may give new information of the material properties of the myocardium.

Combining strain rate imaging with longitudinal M-mode has revealed new information about the physiology and pathophysiology of diastole. It is conceivable that the combination of SRI with one of the three-dimensional techniques will increase the amount of spatio-temporal information.

The method may be improved by increased processing power. In the original paper, strain rate was computed from RF-data, in an off-line application. With acquisition of RF data, both tissue data, velocity and velocity gradients could be computed from the same data set, with optimal frame rate. Whether this will result in reduction of noise, remains to be seen.

6. Conclusions

The study demonstrates that Strain Rate Imaging, by obtaining longitudinal velocity gradients, gives information about regional function of the left ventricle. It is feasible during an ordinary echocardiographic examination. In semi-quantitative assessment of wall motion score, it is comparable to 2D echo in diagnostic accuracy, but with superior temporal resolution. The study has demonstrated that systolic wall thickening and longitudinal wall shortening are equivalent. By corollary, wall thinning and wall elongation during diastole must be related too.

In addition, Strain Rate Imaging gives quantitative measurements of strain rate or strain. Peak systolic strain or strain rate may thus be a method for quantitative stress echo. The accuracy is limited for clinical use at present. The method can also give quantitative measurement of spatio-temporal relations between the different phases and parts of the ventricle.

The study shows new information of diastolic deformation of the ventricle. Diastolic, annular velocities are a function of both magnitude of relaxation rate, as well as the temporal sequence in the ventricle. The filling phases consist of waves of stretching propagation from the base to the apex. Peak strain rate and the propagation velocity of strain rate can describe the two main diastolic events, early and late filling. In reduced diastolic function both are reduced. The velocities of the mitral ring are the result of the combination of this. This adds information about the physiology and pathophysiology of diastole, even though pulsed tissue Doppler is quicker for clinical use. From the information that wall stretching propagates from the base to the apex, as well as the inverse relation between wall thickness and length, a hypothesis of the filling event as a longitudinal process of wall thinning propagation can be established, describing the rate of chamber expansion.

Strain rate propagation in diastole can be seen as a measure of chamber expansion. The decrease in delayed relaxation is consistent with the increased filling time.

Comparing strain rate propagation velocity to flow propagation velocity, flow propagation is not confirmed as a measure of diastolic function, having more determinants than relaxation alone. A relation between flow propagation velocity, flow velocity and, strain rate propagation is conceivable.

Strain Rate Imaging is shown to be more sensitive to both noise and angular distortion than velocity measurement by Doppler tissue imaging.

7. References:

1. Mirsky I and Parmley WW. Assessment of passive elastic stiffness for isolated heart muscle and the intact heart. *Circ. res.* 1973;33(2):233-43
2. Grossman W, Jones D and McLaurin JP. Wall stress and Patterns of Hypertrophy in the Human Left Ventricle. *J Clin Invest* 1975;56:56-64
3. D'hooge J, Heimdal A, Jamal F, Kukulski T, Bijnens B, Rademakers F, Hatle L, Suetens P and Sutherland GR. Regional Strain Rate Measurements by Cardiac Ultrasound: Principles, Implementation and Limitations. *Eur J Echocardiography* (2000)1, 154-70.
4. Lundback S. Cardiac pumping and function of the ventricular septum. *Acta Physiol Scand Suppl* 1986;550:1-101.
5. Assmann PE, Slager CJ, Dreyse ST, van der Borden SG, Oomen JA, Roelandt JR: Two-dimensional echocardiographic analysis of the dynamic geometry of the left ventricle: the basis for an improved model of wall motion. *J Am Soc Echocardiogr* 1988;1:393-405
6. Jones CJ, Raposo L, Gibson DG. Functional importance of the long axis dynamics of the human left ventricle. *Br Heart J* 1990;63:215-20.
7. Alam M, Hoglund C, Thorstrand C. Longitudinal systolic shortening of the left ventricle: An echocardiographic study in subjects with and without preserved global function. *Clin Physiol* 1992;12:443-52
8. Simonson JS, Schiller NB. Descent of the base of the left ventricle: an echocardiographic index of left ventricular function. *J Am Soc Echocardiogr* 1989;2:25-35.
9. Pai RG, Bodenheimer MM, Pai SM, Koss JH, Adamick RD: Usefulness of systolic excursion of the mitral annulus as an index of left ventricular systolic function. *Am J Cardiol* 1991;67:222-4
10. Gulati VK, Katz WE, Follansbee WP, Gorcsan J 3rd Mitral annular descent velocity by tissue Doppler echocardiography as an index of global left ventricular function. *Am J Cardiol* 1996 May 1;77(11):979-84
11. Willenheimer R, Cline C, Erhardt L, Israelsson B. Left ventricular atrioventricular plane displacement: an echocardiographic technique for rapid assessment of prognosis in heart failure. *Heart* 1997;78:230-36.
12. Blomstrand P, Kongstad O, Broquist M, et al. Assessment of left ventricular diastolic function from mitral annulus motion, a comparison with pulsed Doppler measurements in patients with heart failure. *Clinical Physiology* 1996;16:483-93
13. Bojö L, Wandt B, Ahlin N-G. Reduced left ventricular relaxation velocity after acute myocardial infarction. *Clinical Physiology* 1998;18:195-201

14. Rodriguez L, Garcia M, Ares M, et al. Assessment of mitral annular dynamics during diastole by Doppler tissue imaging: Comparison with mitral Doppler inflow in subjects without heart disease and in patients with left ventricular hypertrophy. *Am Heart J* 1996;131:982-7
15. Rademakes FE, Buchalter MB, Rogers WJ, Zerhouni EA, Weisfeldt ML et al. Dissociation between left ventricular untwisting and filling. Accentuation by catecholamines. *Circulation* 1992;85(4):1572-81
16. Fleming D, Xia X, McDicken WN, Sutherland GR, Fenn L. Myocardial velocity gradients detected by Doppler imaging. *Br. J. Radiol.* 1994;799(67):679-88
17. Uematsu M, Miyatake K, Tanaka N et al. Myocardial velocity gradient as a new indicator of regional left ventricular contraction: detection by a 2-dimensional tissue Doppler imaging technique. *J. Am Coll cardiol* 1995;3(25):717-24
18. Wilkenshoff UM, Sovany A, Wigstrom L, Olstad B, Lindstrom L, Engvall J, et al. Regional mean systolic myocardial velocity estimation by real-time color Doppler myocardial imaging: a new technique for quantifying regional systolic function. *J Am Soc Echocardiogr* 1998;11:683-92
19. H. Torp, A. Heimdal, B. Olstad, K. Kristofferson, "Method and apparatus for real-time calculation and display of strain in ultrasound imaging", U.S. patent 6099471, 2000.
20. Heimdal A, D'hooge J, Bijmens B, Sutherland G, Torp H. In vitro validation of in-plane strain rate imaging, a new ultrasound technique for evaluating regional myocardial deformation based on tissue Doppler imaging. *Echocardiography*,15(8 part 2):S40. Abstract.
21. Dahlof B, Devereux R, de Faire U et al. The Losartan Intervention For Endpoint reduction (LIFE) in Hypertension study: rationale, design, and methods. The LIFE Study Group. *Am J Hypertens* 1997 Jul;10(7 Pt 1):705-13
22. Appleton CP, Hatle LK, Popp RL. Relation of transmitral flow velocity patterns to left ventricular diastolic function: new insights from a combined hemodynamic and Doppler echocardiographic study. *J Am Coll Cardiol* 1988 Aug;12(2):426-40 Related Articles, Books, LinkOut
23. Stugaard M. Assessment of diastolic function by colour M-mode Doppler of intraventricular filling. The first diastology meeting, Nice, nov. 28-30, 1996. Published in *heartforum suppl 1-* 1997;10:37-44
24. Schiller NB, Shah PM, Crawford M, et al: Recommendations for quantitation of the left ventricle by two-dimensional echocardiography. *J Am Soc Echocardiogr* 1989, 2:358-67
25. Bjørnstad K, Aakhus S, Lundbom J, Bolz KD, Rokseth R, Skjærpe T, Hatle L. Digital dipyridamole stress echocardiography and upright bicycle stress echocardiography for identification of coronary artery stenosis. *Cardiology* 1995;86:514-20

26. Brodin LA, van der Linden J, Olstad B. Echocardiographic functional images based on tissue velocity information. *Herz* 1998;23:1183-99
27. TIMI Study Group. The thrombolysis in myocardial infarction (TIMI) trial. Phase I findings. *N Engl J Med* 1985;312:932-36
28. Altman DG: Practical statistics for medical research. Chapman & Hall. London 1991: p404.
29. Bland JM, Altman DG. Statistical methods for assessing agreement between two methods of clinical measurement. *Lancet* 1986 Feb 8;1(8476):307-10
30. Alam M, Wardell J, Andersson E et al. Characteristics of Mitral and Tricuspid Annular Velocities Determined by Pulsed wave Doppler Tissue Imaging in Healthy Subjects. *J Am Soc Echocardiogr* 1999;12:618-28
31. Farias CA, Rodrigues L, Garcia MJ et al. Assessment of Diastolic Function by Tissue Doppler Echocardiography: Comparison with Standard Transmitral and Pulmonary Venous Flow. *J Am Soc Echocardiogr* 1999;12:609-17
32. Brun P, Tribouilly C, Duval A-M et al. Left ventricular flow propagation during early filling is related to wall relaxation: A colour M-mode analysis. *J Am Coll Cardiol* 1992;20:420-32
33. Stugaard M, Steen T, Lundervold A et al. Visual assessment of intra ventricular flow from colour M-mode Doppler images. *Int J Cardiac Imaging* 1994;10:279-89
34. Sys SU, Brutsaert DL. Determinants of force decline during relaxation in isolated cardiac muscle. *Am J Physiol* 1989 Nov;257(5 Pt 2):H1490-7
35. Brutsaert DL, Rademakers FE, Sys SU. Triple control of relaxation: implications in cardiac disease. *Circulation* 1984 Jan;69(1):190-6
36. C. Seiler, K. Heule, S. de Marchi Accuracy and preload-dependency of diastolic mitral annular velocity parameters for the assessment of "pseudonormal" left ventricular relaxation Abstract number: 929 *European Heart Journal* Vol 20, Abstr. Suppl. August/September 1999, page 148
37. Voight JU, Lindenmeier G, Cubra A, Werner D, Flaschkampf FA, Hatle L, Sutherland GR. Does strain rate imaging offer new insights into left ventricular function? Abstract, European heart congress Amsterdam august 2000, in: *European heart Journal* 2000,(21), Abstract supplement, p 334, P1795.
38. Urheim S, Edvardsen T, Torp H, Angelsen B, Smiseth OA. Myocardial strain by Doppler echocardiography. Validation of a new method to quantify regional myocardial function. *Circulation* 2000 Sep 5;102(10):1158-64
39. Edvardsen T, Gerber BL, Garot J, Bluemke DA, Lima JAC. Doppler derived strain measures myocardial deformation – validation vs. magnetic resonance tagging. Abstract,

- European heart congress, Amsterdam 2000. in: European heart Journal 2000,(21), August/september , Abstract supplement, 265, p 30.
40. Mele D, Olstad B, Donateo M, Pedini I, Alboni P, Levine RA. Strain Rate Imaging Can Accurately Identify Infarct Segments in Patients With Myocardial Infection: A Clinical Study Abstract, ACC 2000. In: J Am Coll Cardiol 2000, abstract supplement.
 41. A. Abaci, A. Oguzhan, B. Kiranatli, S. Unal, N.K. Eryol, A. Ergin Influence of alteration in preload on the pattern of left ventricular diastolic filling as assessed by Doppler tissue imaging. Abstract number: P1604 European Heart Journal Vol 20, Abstr. Suppl. August/September 1999, page 292
 42. Takatsuji H, Mikami T, Urasawa K, Teranishi J, Onozuka H, Takagi C, Makita Y, Matsuo H, Kusuoka H, Kitabatake A. A new approach for evaluation of left ventricular diastolic function: Spatial and temporal analysis of left ventricular filling flow propagation by colour M-mode Doppler echocardiography. J Am Coll Cardiol 1996;27:365-71.
 43. Steine K, Steine S, Smiseth OA. Slowing of mitral-to-apical flow propagation in the elderly: A colour M-mode Doppler study. Cardiology in the elderly 1996;4:145-9
 44. Slørdahl SA, Bjærum S, Amundsen BA, Støylen A, Heimdal A, Rabben SI, Torp H. High Frame Rate Strain Rate Imaging of the Ventricular Septum in Healthy Subjects. Submitted
 45. Katz AM. Physiology of the heart. 2nd edition. Raven Press, New York 1992:p362.
 46. Hatle L, Angelsen B. Doppler ultrasound in cardiology. Physical principles and clinical applications. 2nd edition. Lea & Febiger, Philadelphia 1985:p 87.
 47. Steen T, Steen S. Filling of a model left ventricle studied by colour M mode Doppler. Cardiovascular research 1994;28:1821-27.
 48. Nagueh SF, Lakkis NM, Middleton KJ, Spencer WH, Zoghbi WA and Quiñones MA. Doppler estimation of left ventricular filling pressures in patients with hypertrophic cardiomyopathy. Circulation. 1999; 99: 254-61.
 49. Houlind K, Schroeder AP, Egeblad H and Pedersen EM. Age-dependent changes in spatial and temporal blood velocity distribution of early left ventricular filling. Magn Reson Imaging 1999 Jul; 17(6): 859-68.
 50. Nagueh SF, Middleton KJ, Kopelen HA, Zoghbi WA, Quinones MA. Doppler Tissue Imaging: a noninvasive technique for evaluation of left ventricular relaxation and estimation of filling pressures. J Am coll cardiol 1997; 30: 1527-33.
 51. Garcia MJ, Smedira NG, Greenberg NL, Main M, Firstenberg MS, Odabashian J, Thomas J. Color M-mode Doppler flow propagation is a preload insensitive index of left ventricular relaxation: animal and human validation. J Am Coll Cardiol 2000 Jan; 35(1): 201-8.

52. Kvitting JP, Wigstroem L, Strotmann JM, Sutherland GR. How accurate is of visual assessment of synchronicity in myocardial motion? An in vitro study with computer-simulated regional delay in myocardial motion: Clinical implication for rest and stress echocardiography studies. *J Am Soc Echocardiogr*, 1999, 12: 698-705
53. F. Jamal, T. Kukulski, J. D'hooge, I. De Scheerder and G. Sutherland, "Abnormal postsystolic thickening in acutely ischemic myocardium during coronary angioplasty: A velocity, strain, and strain rate Doppler myocardial imaging study", *Journal of the American Society of Echocardiography*, vol 12, no 11, pp. 994-996, 1999.
54. A Støylen, T Skjærpe, A Heimdal. Post-systolic shortening in myocardial infarction. A study using Strain Rate Imaging by ultrasound. European Heart Congress Amsterdam 2000. Abstract number P674. In *European heart journal* 2000(21), august/september Abstract suppl., 111.
55. Cain P, Case C, Marwick T. Quantitation of the long axis during stress echo – which marker can best predict presence of coronary artery disease.
56. Andreas Heimdal: Chapter 5: Angle dependency of strain rate pp 55 – 64 in: *Doppler based ultrasound imaging methods for non-invasive assessment of viability*. Trondheim, September 1999
57. Støylen A, Skjærpe T: Lack of regional information from systolic longitudinal motion and velocity of the mitral annulus. Comparison with strain rate imaging. Abstract. Submitted to European Heart Congress 2001.

Appendix: Mathematics of strain and strain rate:

Strain and strain rate:

One-dimensional strain of a body is defined as:

$$1a) \quad \text{Lagrangian strain:} \quad \epsilon = \frac{L - L_0}{L_0} = \frac{\Delta L}{L_0}$$

$$1b) \quad \text{Natural strain:} \quad \epsilon' = \ln \left(\frac{L}{L_0} \right)$$

Where L_0 is the length at time t_0 ($t_0 = 0$), and L is the length at time t ($L = L(t)$). It follows from the definitions that strain is dimensionless, but also that positive strain is lengthening or stretching, negative strain is shortening or compression. But from this:

$$2a) \quad \ln(\epsilon) = \ln \left(\frac{L - L_0}{L_0} \right) = \ln \left(\frac{L}{L_0} - \frac{L_0}{L_0} \right) = \ln \left(\frac{L}{L_0} - 1 \right)$$

$$2b) \quad \ln(\epsilon + 1) = \ln \left(\frac{L}{L_0} \right)$$

And thus:

$$3a) \quad \epsilon = e^{\epsilon'} - 1$$

$$3b) \quad \epsilon' = \ln(\epsilon + 1)$$

Strain rate, the rate of change, is strain per time unit:

$$4) \quad \dot{\epsilon} = \frac{d\epsilon}{dt}$$

From the formula, it is evident that the unit of strain rate, is s^{-1} . The instantaneous change in strain (strain increment or decrement is:

$$\text{For Lagrangian strain: as} \quad \epsilon = \frac{L - L_0}{L_0} = \frac{L}{L_0} - \frac{L_0}{L_0} = \frac{L}{L_0} - 1, \text{ then}$$

$$\frac{d\epsilon}{dL} = \frac{1}{L_0} \text{ and thus}$$

$$5a) \quad d\epsilon = \frac{dL}{L_0}$$

$$\text{For Natural strain: as} \quad \epsilon' = \ln \left(\frac{L}{L_0} \right) = \ln(L) - \ln(L_0) \text{ and } L_0 \text{ is constant, so is}$$

$$\ln(L_0). \text{ Then} \quad \frac{d\epsilon'}{dL} = \frac{1}{L} \text{ and thus}$$

$$5b) \quad d\epsilon' = \frac{dL}{L}$$

Thus Lagrangian strain change uses original length as a reference, while natural strain change uses instantaneous length, in other words the reference length changes as a function of time. Natural strain is independent of the definition of the reference length.

The instantaneous change in length is:

$$6) \quad dL = L(t+dt) - L(t)$$

for both Lagrangian and natural strain.

The velocity gradient.

For an object undergoing strain, the length change is related to the velocity gradient. The myocardial velocity gradient means velocity difference per length unit. It was originally defined as the velocity gradient across the wall (15):

$$7) \quad VG = - \frac{dr/dt}{r} = - \frac{\Delta v}{r}$$

where r is the instantaneous wall thickness. The unit of the velocity gradient is cm/s/cm , which is equal to s^{-1} . The gradient was found as the slope of the linear regression of the tissue velocities. (The linear regression assumes that the velocity distribution is homogenous.) The velocity gradient is thus equal to:

$$8) \quad VG = - \frac{\Delta v}{r} = - \frac{(v_1 - v_2)}{r} = \frac{(v_2 - v_1)}{r},$$

under the assumption that the velocity gradient is constant over the length r (spatially homogenous). In fact, by this assumption, the velocity gradient can be obtained by the endocardial and epicardial traces which gives the thickness r , as well as the velocities by derivation. The velocity regression, however, is less noise sensitive. For an object undergoing longitudinal strain, we can replace r with L , where L is the instantaneous length of the object. By this, the longitudinal velocity gradient is:

$$9a) \quad VG = \frac{(v_2 - v_1)}{L} = \frac{dL/dt}{L}$$

$$9b) \quad dL = (v_1 - v_2) dt$$

This gives:

$$10a) \quad d\varepsilon = \frac{dL}{L_0} = \frac{(v_2 - v_1)}{L_0} dt$$

$$10b) \quad d\varepsilon' = \frac{dL}{L} = \frac{(v_2 - v_1)}{L} dt$$

And thus:

$$11a) \quad \dot{\varepsilon} = \frac{(v_2 - v_1)}{L_0}$$

$$11b) \quad \dot{\epsilon}' = \frac{(v_2 - v_1)}{L}$$

In other words, the natural strain rate is equal to the velocity gradient.

Strain by integrated strain rate.

For an object undergoing strain from t_0 to t or alternatively from L_0 to L , this means, that strain can be described as the integral of strain rate. By integrating equations 10a) and 10b):

$$12a) \quad \epsilon = \int_{t_0}^t d\epsilon = \int_{L_0}^L \frac{dL}{L} = \int_{t_0}^t \frac{(v_2 - v_1)}{L_0} dt$$

$$12b) \quad \epsilon' = \int_{t_0}^t d\epsilon' = \int_{L_0}^L \frac{dL}{L} = \int_{t_0}^t \frac{(v_2 - v_1)}{L} dt$$

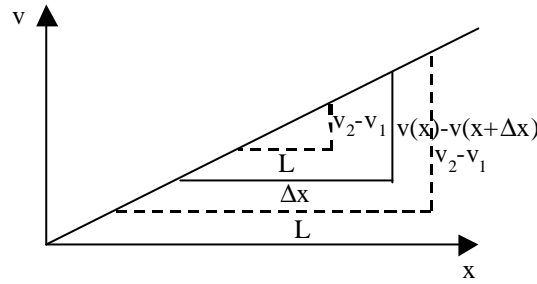
Strain and strain rate by tissue Doppler.

In colour tissue Doppler, the velocities of all pixels are sampled simultaneously. The strain rate is sampled as the velocity gradient with a fixed offset distance Δx . As there is no tracking of the endpoints of the initial length (object), neither the velocities nor the distance relates directly to the strain of a defined object. We do not measure the instantaneous length change, nor the velocities at the endpoints. The strain rate estimator is thus (fig. 6):

$$13) \quad SR = \frac{v(x) - v(x + \Delta x)}{\Delta x}$$

If the instantaneous length L at a certain time coincides with Δx , $v(x) = v_2$ and $v(x + \Delta x) = v_1$.

Then SR equals natural strain rate ($\dot{\epsilon}'$) in equation 11b). Usually, however, L will differ from Δx , for most frames and objects, and the velocities will hence differ too. Under the assumption that the strain is equally distributed over the length of the object (spatially constant), SR will still be equal to natural strain rate. Strain being spatially constant means that the velocity increases linearly along the length as shown in the diagram:



For any L that is different from Δx , $v_2 - v_1$ will be greater or smaller than $v(x) - v(x + \Delta x)$ by the same ratio. In the figure, this is evident, as the slope of the curve is the same wherever it is measured. As v_1 and v_2 are the velocities of the end points of L , the ratio in equation 13) will always be the same as the ratio in 11b):

$$SR = \dot{\epsilon}'$$

It is also evident that as L_0 is constant, the ratio in equation in 11a) will only be equal to 13) when $\Delta x = L_0$, and this will always change from one frame to next. Thus:

$$SR \neq \dot{\epsilon}.$$

The argument and equation 13) is simplified in relation to the algorithm implemented in the computer. Velocities are measured by the autocorrelation method, by analysing the phase shifts of the reflected signals. The online strain rate is measured directly by autocorrelation as well, as discussed by Heimdal (56).

The integral of SR will then give natural strain:

$$15) \quad \epsilon' = \int_{t_0}^t SR dt$$

Lagrangian strain can then be estimated by

$$16) \quad \epsilon = e^{\epsilon'} - 1 = \exp\left(\int_{t_0}^t SR dt\right) - 1$$

which can be implemented in the processing software.

5. Strain in more than one dimension:

The discussion above is limited to one-dimensional strain. In two dimensions (Fig. 2), there are four strain components. Two normal strains:

$$17) \quad \epsilon_x = \frac{\Delta x}{x} \quad \text{and} \quad \epsilon_y = \frac{\Delta y}{y}$$

and two shear strains:

$$18) \quad \epsilon_{xy} = \frac{\Delta x}{y} \quad \text{and} \quad \epsilon_{yx} = \frac{\Delta y}{x}$$

From Fig. 2, it is also obvious that

$$19) \quad \epsilon_{xy} = \tan \alpha_x \quad \text{and} \quad \epsilon_{yx} = \tan \alpha_y$$

All strain components can be written in a matrix, the strain tensor:

$$20) \quad \begin{matrix} \epsilon_x & \epsilon_{xy} \\ \epsilon_{yx} & \epsilon_y \end{matrix}$$

For a homogenous, isotropic and incompressible object, $\epsilon_{xy} = \epsilon_{yx}$.

In three dimensions, three normal and six shear strains can be defined:

$$21) \quad \begin{matrix} \epsilon_x & \epsilon_{xy} & \epsilon_{xz} \\ \epsilon_{yx} & \epsilon_y & \epsilon_{yz} \\ \epsilon_{zx} & \epsilon_{zy} & \epsilon_z \end{matrix}$$

But as illustrated in fig. 2, the components are interrelated by incompressibility.

6. Angle dependency of strain and strain rate measurement

This is illustrated in fig. 17. Δv is measured along the ultrasound beam. The measured longitudinal velocity is reduced by the cosine of the angle α between the longitudinal velocity vector and the ultrasound beam, $\Delta v_{lm} = \Delta v_l * \cos(\alpha)$. In addition there is a transverse velocity difference, where $\Delta v_{tm} = \Delta v_t * \cos(\beta)$ when measured along the same ultrasound beam. The total measured velocity difference is thus the sum of the two:

$$22) \quad \Delta v_m = \Delta v_l * \cos(\alpha) + \Delta v_t * \cos(\beta)$$

The offset distance, however, is measured as the length of the projection along the ultrasound beam as well, and this increases by the cosine of α :

$$23) \quad \Delta x_m = \frac{\Delta x_l}{\cos(\alpha)} = \frac{\Delta x_t}{\cos(\beta)}$$

The measured strain rate is thus ($\cos(\beta) = \sin(\alpha)$):

$$24) \quad SR_m = \frac{\Delta v_m}{\Delta x_m} = \frac{\Delta v_l}{\Delta x_l} * \cos^2(\alpha) + \frac{\Delta v_t}{\Delta x_t} * \cos^2(\beta)$$

$$25) \quad SR_m = SR_l * \cos^2(\alpha) + SR_t * \cos^2(\beta) = SR_l * \cos^2(\alpha) + SR_t * \sin^2(\alpha)$$

The incompressibility of heart muscle (conservation of volume) means in two dimensions:

$$26) \quad SR_l + SR_t = 0 \Leftrightarrow SR_l = -SR_t$$

Thus:

$$27) \quad SR_m = SR_l * (\cos^2(\alpha) - \sin^2(\alpha))$$